Accepted Article

Title: Electronic Structure of trans-[VII(E(CH3)2CH2CH2E(CH3)2)2], E = N, P

Authors: Mehrafshan G. Jafari, Eva M. Zolnhofer, Dominik Fehn, Frank W. Heinemann, Adedemola A. Opalade, Patrick J. Carroll, Karsten Meyer, J. Krzystek, Andrew Ozarowski, Daniel J. Mindiola, Timothy A. Jackson, and Joshua A. Telser

WILEY▪VCH

Electronic Structure of
trans-[V^{II}(E(CH$_3$)$_2$CH$_2$CH$_2$E(CH$_3$)$_2$)$_2$], E = N, P

Mehrafshan G. Jafari,[¶] Eva M. Zolnhofer,[€] Dominik Fehn,[€] Frank W. Heinemann,[€]
Adedemola A. Opalade,[†] Patrick J. Carroll,[¶] Karsten Meyer,[€] J. Krzystek,[¥] Andrew Ozarowski,[¥]
Daniel J. Mindiola,[¶]* Timothy A. Jackson,[†]* and Joshua Telser[⊥]*

[¶]*Department of Chemistry, University of Pennsylvania, Philadelphia, Pennsylvania 19104, United States*
[€]*Department of Chemistry and Pharmacy, Inorganic Chemistry, Friedrich-Alexander-Universität Erlangen-Nürnberg (FAU), 91058 Erlangen, Germany.*
[¥]*National High Magnetic Field Laboratory, Florida State University, Tallahassee, Florida 32310, United States.*
[†]*Department of Chemistry, University of Kansas, 1567 Irving Hill Road, Lawrence, Kansas 66045, United States.*
[⊥]*Department of Biological, Physical and Health Sciences, Roosevelt University, Chicago, Illinois 60605, United States.*

*Corresponding Authors:

Daniel J. Mindiola: mindiola@sas.upenn.edu
Timothy A. Jackson: taj@ku.edu
Joshua Telser: jtelser@roosevelt.edu

1

Abstract

Coordination complexes of general formula *trans*-[MX$_2$(R$_2$ECH$_2$CH$_2$ER$_2$)$_2$] (M^{II} = Ti, V, Cr, Mn; E = N or P; R = alkyl or aryl) are a cornerstone of coordination and organometallic chemistry. We investigate the electronic properties of two such complexes, *trans*-[VCl$_2$(tmeda)$_2$] and *trans*-[VCl$_2$(dmpe)$_2$], which thus represent *trans*-[MX$_2$(R$_2$ECH$_2$CH$_2$ER$_2$)$_2$] where M = V, X = Cl, R = Me and E = N (tmeda) and P (dmpe). These V^{II} complexes have S = 3/2 ground states, as expected for octahedral d^3. Their tetragonal distortion leads to zero-field splitting (zfs) that is modest in magnitude ($D \approx 0.3$ cm^{-1}) relative to analogous S = 1 Ti^{II} and Cr^{II} complexes. This parameter was determined from conventional EPR spectroscopy, but more effectively from high-frequency and -field EPR (HFEPR) that determined the sign of D as negative for the diamine complex, but positive for the diphosphine, which information had not been known for any *trans*-[VX$_2$(R$_2$ECH$_2$CH$_2$ER$_2$)$_2$] systems. The ligand-field parameters of *trans*-[VCl$_2$(tmeda)$_2$] and *trans*-[VCl$_2$(dmpe)$_2$] are obtained using both classical theory and *ab initio* quantum chemical theory. The results shed light not only on the electronic structure of V^{II} in this environment, but also on differences between N and P donor ligands, a key comparison in coordination chemistry.

Keywords

2

Introduction

Chelating ligands, $R_2E(CH_2)_nER_2$, (E = Group 15 donor; $n = 1 – 3$, R = H, alkyl, aryl), play an important and historical role in coordination and organometallic chemistry. The size of the chelate ring is controlled by n, wherein $n = 2$ forms the more stable five-membered metal-chelate ring and as such, this scaffold is the most commonly employed. The σ-donor and π-acceptor properties of E are controlled by Period, with E = N being the classical coordination chemistry ligand (e.g., R = H gives ethane-1,2-diamine, en) with no π-bonding and E = P being the classical organometallic ligand series (e.g., R = Me giving dmpe, 1,2-bis(dimethylphosphino)ethane, R = Et giving depe, 1,2-bis(diethylphosphino)ethane, and R = Ph giving dppe, 1,2-bis(diphenylphosphino)ethane) with π-acceptor properties. In a landmark manuscript, Girolami, Wilkinson, and co-workers reported a series of first-row divalent transition metal dmpe complexes of general formula *trans*-$[MX_2(Me_2PCH_2CH_2PMe_2)_2]$, where M^{II} = Ti, V, Cr, Mn, and X = Me, Cl, Br.[1] Not every permutation was prepared: for X = Cl, M = Ti, V, Cr; for X = Br and I, M = Mn; for X = Me, M = Ti (but with residual chloride; formula: $Me_{1.3}Cl_{0.7}$), V, Cr, Mn. The complex where M = Cr, X = Me had also been reported in an earlier communication.[2] Subsequent studies by Girolami and co-workers explored the chemistry of *trans*-$[TiX_2(Me_2PCH_2CH_2PMe_2)_2]$, X = Me,[3] OPh,[4] η^2-BH_4,[5] Previously reported complexes of Ti^{II} with the same tetragonal geometry,[6] but with nitrogen donor ligands, have been recently explored by us. These are *trans*-$[TiCl_2(py)_4]$ (py = pyridine),[7] and *trans*-$[TiCl_2(tmeda)_2]$ (tmeda = N,N,N',N'-tetramethylethane-1,2-diamine = $Me_2NCH_2CH_2NMe_2$).[8] As an aside on the vagaries of nomenclature, tmeda and dmpe are both $Me_2ECH_2CH_2EMe_2$ (E = N and P, respectively), yet have common names that originate respectively in coordination chemistry and in organometallic chemistry, and thus seem more different structurally than they are. A theme that is pervasive in these studies, and of importance for practical applications,[9] is the variation in spin ground state among related complexes. For example, the spin ground state of *trans*-$[TiX_2(dmpe)_2]$ is a function of axial ligand, wherein X = Cl^- [1] and η^2-BH_4^- [5] have the triplet ground state expected for d^2, but for X = Me^- [3] and PhO^- [4] the ground state is a singlet (diamagnetic). As discussed by Girolami and co-workers, this is rather counter intuitive as one would anticipate the half-filled e_g set (d_{xz}, d_{yz}) in a pseudo D_{4h} symmetric system to be degenerate or very close in energy.

3

In the case of the V^{II} congeners, the subject of the present study, *trans*-[$VX_2(Me_2ECH_2CH_2EMe_2)_2$] where X = Cl, Br, I; E = N, P,[1, 10] the spin ground state is the expected $S = 3/2$. This quartet ground state is also found for the corresponding V^{II} complexes with axial alkyl ligands, *trans*-[$VMe_2(dmpe)_2$][1] and *trans*-[$V(CH_2SiMe_3)_2(dmpe)_2$],[11] and for *trans*-[$V(\eta^1\text{-}BH_4)_2(dmpe)_2$].[5] The cationic complexes *trans*-[$V(NCMe)_2(dmpe)_2$](BPh_4)$_2$ and *trans*-[$V(CN^tBu)_2(dmpe)_2$](PF_6)$_2$, which were structurally characterized by Anderson et al.[12], along with others of formula *trans*-[$VL_2(dmpe)_2$]$^{0,2+}$ that were not, all had quartet ground states. Other complexes of general formula *trans*-[$VX_2(R_2PCH_2CH_2PR_2)_2$] (X = Cl⁻, Br⁻, I⁻; R = Me, Et, Ph) were studied by Leigh and co-workers including their electronic absorption spectra.[10b] The electronic absorption spectra of the series *trans*-[$VX_2(dmpe)_2$] (X = Cl⁻, Br⁻, I⁻, Me⁻, and $CF_3SO_3^-$) was extensively studied by Taube and co-workers.[13] They also investigated many complexes of V^{II} with only monodentate ligands, chiefly pyridine (py), of general formula *trans*-[$VX_2(py)_4$] (X = Cl⁻, Br⁻, I⁻, SCN⁻, N_3^-, PhS⁻, EtS⁻, BH_4^-, and $CF_3SO_3^-$.[13-14] More recently, Shores and co-workers have studied V^{II} (and Cr^{III}) complexes including using computational methods unavailable to earlier studies.[15] Notably, they found a doublet ground state for a V^{II} complex, although this was the consequence of a non-innocent tripodal iminopyridyl ligand.[15a]

As part of our interest in applying electron paramagnetic resonance (EPR) spectroscopy to 3d complexes with $S > 1/2$ ground states, and in particular using high-frequency and -field EPR (HFEPR) to determine definitively the magnitude and sign of the zero-field splitting (zfs) in such systems,[16] we apply these methods to *trans*-[$VCl_2(Me_2ECH_2CH_2EMe_2)_2$] (E = N and P) . We use classical ligand-field theory (LFT) to analyze these two complexes, as was done previously for several V^{II} bisdiamine complexes,[17] We also use quantum chemical theory (QCT), specifically *ab initio* methods that were unavailable in earlier studies. We note a pioneering QCT study that applied intermediate neglect of differential overlap (INDO) methods to *trans*-[$VCl_2(tmeda)_2$].[18] Our results provide a comprehensive picture of the electronic structure of the *trans*-[$VCl_2(Me_2ECH_2CH_2EMe_2)_2$] system as well as of related complexes, shedding light in particular on the difference between the N and P donor ligands, which is of general importance in the realm of coordination chemistry.

4

Experimental Section

General considerations. Manipulation of air-sensitive compounds was performed using standard Schlenk-line techniques or an MBraun inert-gas glovebox containing an atmosphere of purified dinitrogen or argon where specified. Solvents were purified using a two-column solid-state purification system (Glasscontour System, Joerg Meyer, Irvine, CA), transferred to the glovebox without exposure to air and stored over activated molecular sieves and/or sodium metal. NMR solvents were dried over Na/K alloy or molecular sieves and distilled under reduced pressure and/or filtered through a column of neutral activated aluminum oxide. Elemental analysis results were obtained from the Analytical Laboratories at FAU-Erlangen-Nürnberg, using Euro EA 3000 (Euro Vector) and EA 1108 (Carlo-Elba) elemental analyzers. Electronic absorption spectra were recorded on a Shimadzu UV-3600 UV-vis-NIR spectrophotometer in toluene solution at room temperature.

Synthesis. The procedure of Girolami *et al*. was used for synthesis of *trans*-[VCl$_2$(dmpe)$_2$][1] and that of Edema *et al*. for *trans*-[VCl$_2$(tmeda)$_2$].[10a]

X-Ray Crystallography. Details of the X-ray crystallography of *trans*-[VCl$_2$(tmeda)$_2$] and *trans*-[VCl$_2$(dmpe)$_2$], each collected at 100 K, are given in Supporting Information Section S1 including additional figures (S1 – S5). Figures S3 and S5, respectively, show the crystal packing diagram for each complex, demonstrating that there are no intermolecular interactions.

Conventional (X- and Q-band) EPR and ENDOR Spectroscopy. X-band EPR spectra were recorded on a modified Bruker E-109 spectrometer equipped with an Oxford cryostat. Continuous wave (CW) Q-band (35 GHz) EPR and ENDOR spectra were recorded at 2 K on a spectrometer described elsewhere.[19] CW EPR spectra under the employed conditions are in some cases in rapid passage[20] and thus exhibit an absorption lineshape.

High-Frequency and -Field EPR Spectroscopy (HFEPR). HFEPR data were acquired at the EMR Facility of the NHMFL using a spectrometer previously described,[21] but modified by the use of low-frequency sources followed by a chain of amplifiers and frequency multipliers (VDI Inc., Charlottesville, VA, USA), which operate in the frequency range of 50 – 420 GHz. The programs QPOW,[22] DDPOWH (J. Telser), and SPIN (A. Ozarowski) were variously used for EPR simulations.

5

Computational Methods. Ligand Field Theory (LFT) calculations employed the locally written (J. Telser) programs DDN and DDNFIT and the program Ligfield by J. Bendix.[23] All Quantum Chemical Theory (QCT) calculations were performed using ORCA 5.03[24] Details are provided in the Supporting Information, Sections S5 (LFT) and S6 (QCT), respectively.

Results and Discussion

Crystal Structures of V^{II} complexes with $Me_2ECH_2CH_2EMe_2$ ligands. The crystal structures of *trans*-[VCl$_2$(dmpe)$_2$] and *trans*-[VCl$_2$(tmeda)$_2$] were respectively and previously reported by Girolami *et al.* (CSD code: DAJDUN)[1] and by Edema *et al.* (CSD code: VERJEH).[10a] Both structures had been determined at room temperature, so low temperature (100 K) structures were determined here for overall confirmation as well as better comparison with low temperature, solid-state (HF)EPR spectroscopy and computational studies. The structures are shown together in Figure 1 and separately in Figures S1 and S4 (Supporting Information), respectively. The structural disorder in the case of *trans*-[VCl$_2$(tmeda)$_2$] is shown in Figure S2. The crystal packing is shown for the two complexes, respectively, in Figures S3 and S5. Crystallographic information is given in Table S1. The differences between the previous room temperature and the current 100 K structures are minimal. Supporting Information Section S2, Table S2 summarizes the relevant metrics for a wide series of complexes of general formula *trans*-[VX$_2$(R$_2$ECH$_2$CH$_2$ER$_2$)$_2$]$^{0,2+}$, where R = Me, Et, Ph, and X = a wide range of monoanionic ligands, primarily, but not exclusively halides.
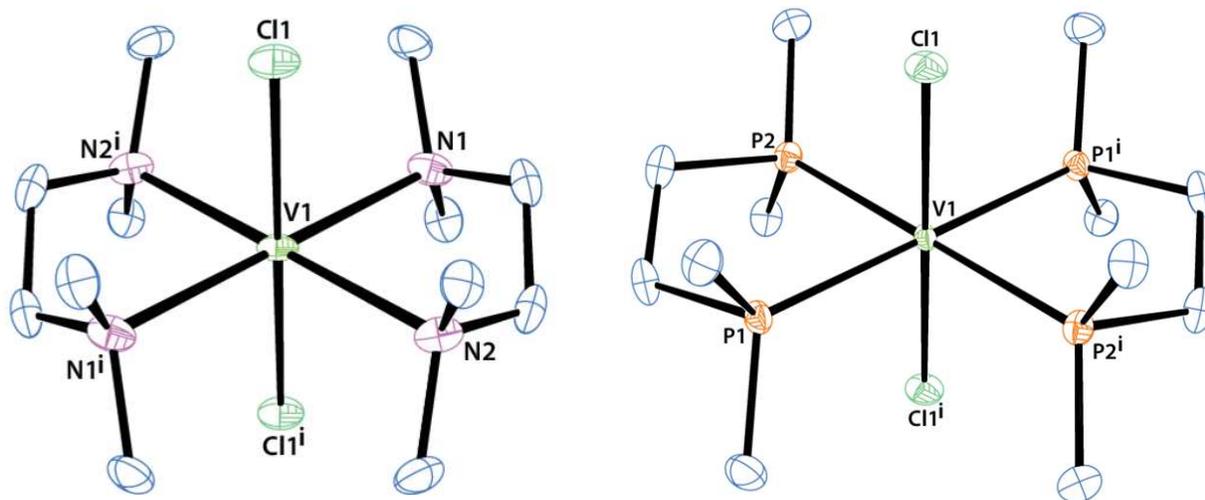
Figure 1. Molecular structures of *trans*-[VCl$_2$(tmeda)$_2$] (left) and *trans*-[VCl$_2$(dmpe)$_2$] (right). Thermal ellipsoids are drawn at 50% probability and H atoms are omitted for clarity. Disorder in one tmeda ligand is not shown for clarity. Only molecule 1 of the two crystallographically independent (but chemically equivalent) molecules is shown for *trans*-[VCl$_2$(dmpe)$_2$]. See Figures S1 – S5 (Supporting Information) for further crystal structure representations.

The relevant, averaged metrics (in Å) from the current, low temperature structures are: *trans*-[VCl$_2$(tmeda)$_2$], d(V-Cl) = 2.4878(2), d(V-N) = 2.3185(8); *trans*-[VCl$_2$(dmpe)$_2$], d(V-Cl) = 2.4419(4), d(V-P) = 2.4952(4).[25]   The key crystallographic feature for the present purposes of electronic structure analysis is the same as that in the complexes previously studied by us, *trans*-[TiCl$_2$(tmeda)$_2$][8] and *trans*-[CrCl$_2$(dmpe)$_2$];[26] namely, that the Cl-M-Cl angle is 180° and that ∠Cl-M-E (M = V, E = N, P here) average to 90° (with a range of only ±0.1° for E = N and ±2° for E = P). Thus, a tetragonally distorted octahedral coordination describes these V^{II} complexes well, which was the case for the Ti^{II} and Cr^{II} congeners. The chelation of Me$_2$ECH$_2$CH$_2$EMe$_2$ (E = N, P) leads to a slight orthorhombic distortion (∠E-V-E < 90°; 81.45° for E = N and 81.66° for E = P), so that the idealized molecular point group symmetry of the inner coordination sphere is D_{2h}, and taking into consideration the ethylene backbone of the chelates the symmetry is only C_i. However, for the purposes of a simple LFT analysis, D_{4h} symmetry is generally sufficient, with D_{2h} being used for QCT as will be discussed below.

Electronic Absorption Spectroscopy. The electronic absorption spectra recorded in toluene solution at room temperature for the two complexes are shown in Figure 2. Despite both being essentially octahedral complexes of V^{II} with *trans*-Cl$_2$E$_4$ (E = N, P) donor sets, the two spectra are markedly different. The diphosphine complex exhibits no absorption in the NIR region and much higher molar absorption coefficients in the visible and UV regions. Assignments of the bands observed for the two complexes will be made below in the LFT and QCT sections. Supporting Information Section S3, Table S3 summarizes electronic absorption data that have been reported for complexes of general formula *trans*-[VX$_2$(RR′ECH$_2$CH$_2$ERR′)$_2$] (E = N, P; X = halides and other anionic ligands).[10b, 13, 17]

There are notable differences among the electronic absorption spectra in tetrahydrofuran (THF) solution of *trans*-[VCl$_2$(tmeda)$_2$] and other closely related complexes as reported by

7

Niedwieski *et al.* [17] (see Table S3). Specifically, spectra in the visible region of [VCl$_2$(dmeda)$_2$] and [VCl$_2$(deeda)$_2$] were blue-shifted from those of [VCl$_2$(tmeda)$_2$] and [VCl$_2$(dieda)$_2$].[27] The relation between this observation and the ligand-field of these complexes was discussed by Niedwieski *et al.* [17] and will be noted below in the LFT section. It is also apparent that the spectrum of *trans*-[VCl$_2$(tmeda)$_2$] is red-shifted in the non-polar solvent toluene compared to that in the polar solvent THF. In the case of *trans*-[VCl$_2$(dmpe)$_2$], there is a slight blue shift in toluene (and in the solid, by diffuse reflectance[10b]) compared to that in the polar solvent dichloromethane (DCM).
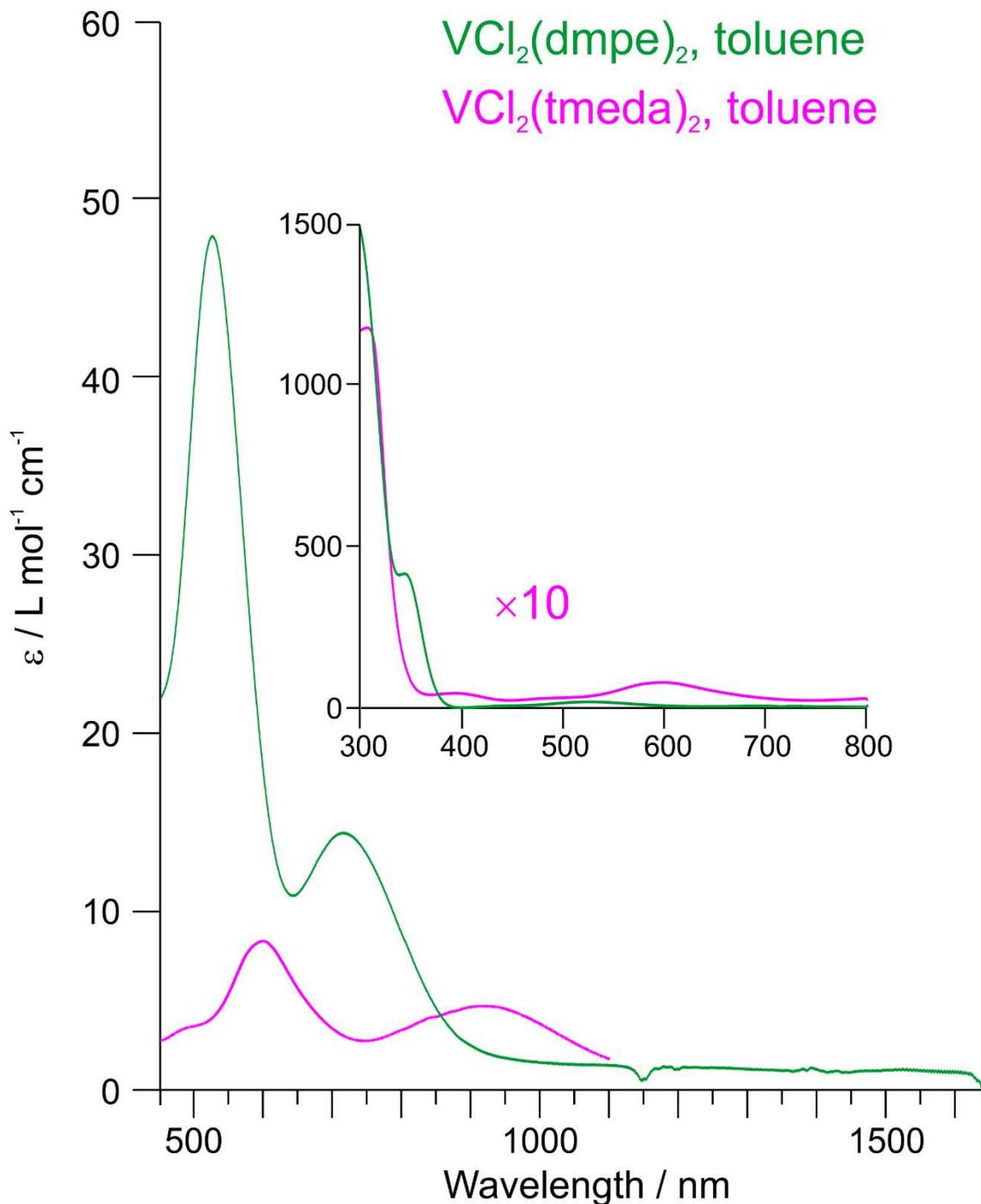
Figure 2. Electronic absorption spectra of *trans*-[VCl$_2$(tmeda)$_2$] (magenta traces) and *trans*-[VCl$_2$(dmpe)$_2$] (green traces) in toluene solution at room temperature. The main figure shows the visible and NIR regions and the inset shows the UV and visible regions. The ordinate is in molar absorption coefficient in all cases and is scaled by 10× for the tmeda complex in the inset.

9

Conventional (X- and Q-band) EPR spectroscopy. The X-band EPR spectrum in frozen toluene/THF (1:1 v/v) solution (4 K) for *trans*-[VCl$_2$(tmeda)$_2$] is shown in Figure 3. The simulation neglects hyperfine coupling (hfc) from ^{51}V ($I = 7/2$, ~100% abundance), which is partially resolved in the z_1 and z_3 transitions (i.e., those at the field extrema), using the nomenclature standard for a spin quartet.[28] Figure 4 presents expansions of the z_1 and z_3 transitions with simulations that include ^{51}V hfc, yielding $A_z(^{51}\text{V}) = 210$ MHz. In this case, the simulation linewidths are narrow so that the ideal hfc pattern is evident and that it matches the resolved features of the experimental spectrum in these field regions. It is impossible to determine the ^{51}V hfc at x and y transitions, but the linewidth of the central region ($x_{1,2,3}$, $y_{1,2,3}$, and z_2 transitions – substantially overlapped) suggests that the ^{51}V hfc is similar to that at z_1 and z_3. Q-band spectra of *trans*-[VCl$_2$(tmeda)$_2$] recorded at 2 K are shown in Figures S6 and S7, with the latter being an expansion showing partially resolved ^{51}V hfc analogous to that seen at X-band (Figure 4). QCT calculations described below give an idea as to the full $\mathbf{A}(^{51}\text{V})$ tensor.

The X-band EPR spectrum in frozen DCM solution (77 K) for *trans*-[VCl$_2$(tmeda)$_2$] has been previously reported by Niedwieski *et al.*[18] Their spectrum is qualitatively similar to that shown in Figure 3. These workers reported effective (i.e., $S' = 1/2$) g values of $g'_\perp = 3.68$ and $g'_\parallel = 1.89$. The corresponding features in Figure 3 are at $g'_\perp = 4.24 - 3.42$ (depending on whether the signal maximum or baseline crossover is selected) and $g'_\parallel = 1.98$. These differences may be due to the choice of solvent, as also manifest by the variation in optical spectral described above. In any case, it appears from X-band EPR that for *trans*-[VCl$_2$(tmeda)$_2$] $|D| = 0.25(1)$ cm^{-1}, with a small rhombic component, $|E| = 0.014(5)$ cm^{-1}.

10
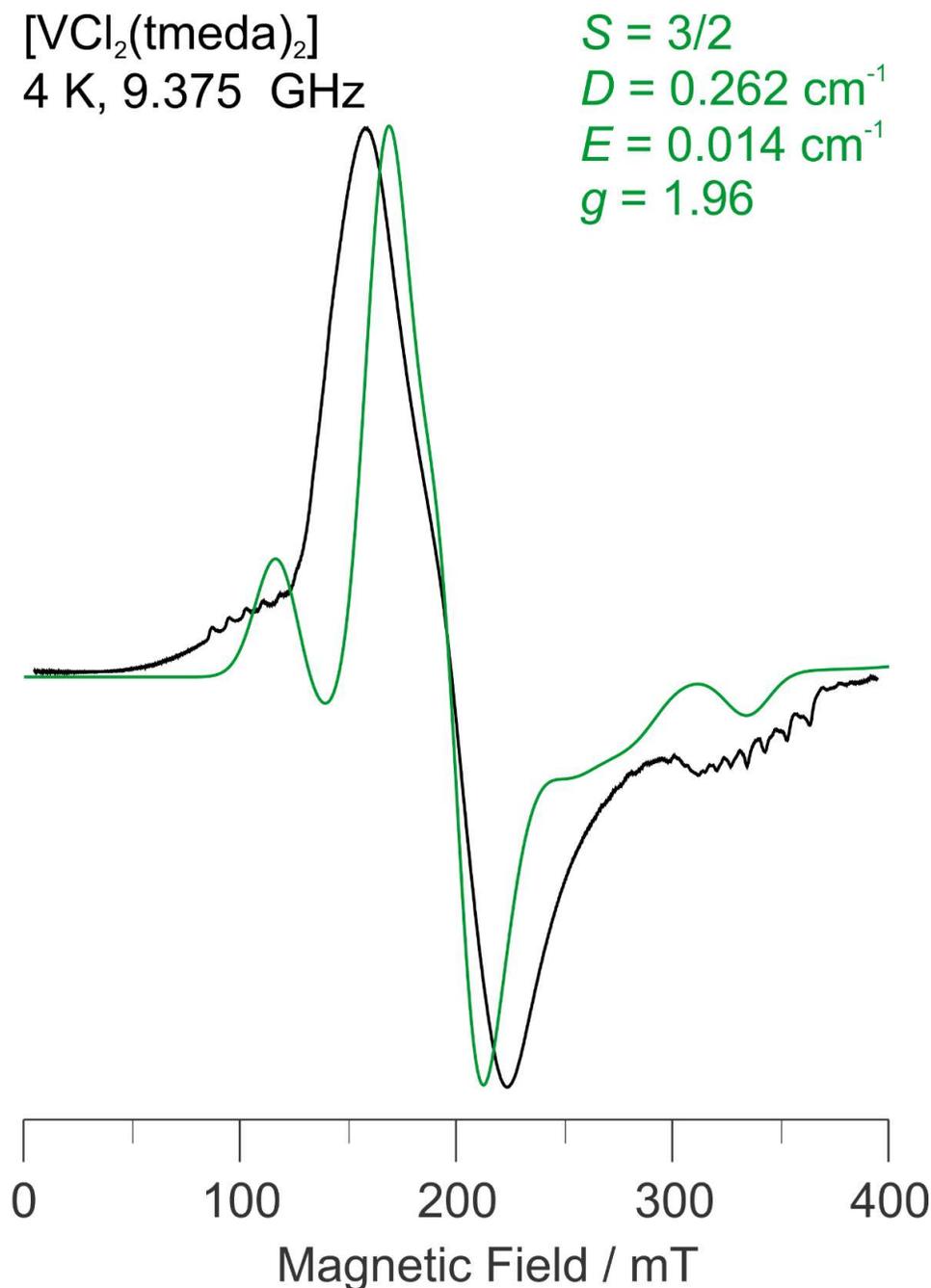
Figure 3. X-band EPR spectrum of *trans*-[VCl$_2$(tmeda)$_2$] (black trace) recorded in toluene/THF (1:1 v/v) frozen solution at 4 K and 9.375 GHz with 100 kHz field modulation amplitude of 1 mT; time constant, 320 ms; 90 s scan. Simulation (green trace) uses: $S = 3/2$, $D = 0.262$ cm^{-1}, $E = 0.014$ cm^{-1}, $g_{iso} = 1.96$, Gaussian linewidths of 10 mT. Hyperfine coupling from ^{51}V is seen at the field extrema (z_1, low field; z_3, high field) and contributes to the spectral width in the central region (~200 mT), but is not simulated. As a result, the simulation does not match the central lineshape exactly and matches only the centers of the z_1 and z_3 features. Figure 4 shows an analysis of hyperfine effects. See Figures S6 and S7 for Q-band EPR spectra.

11
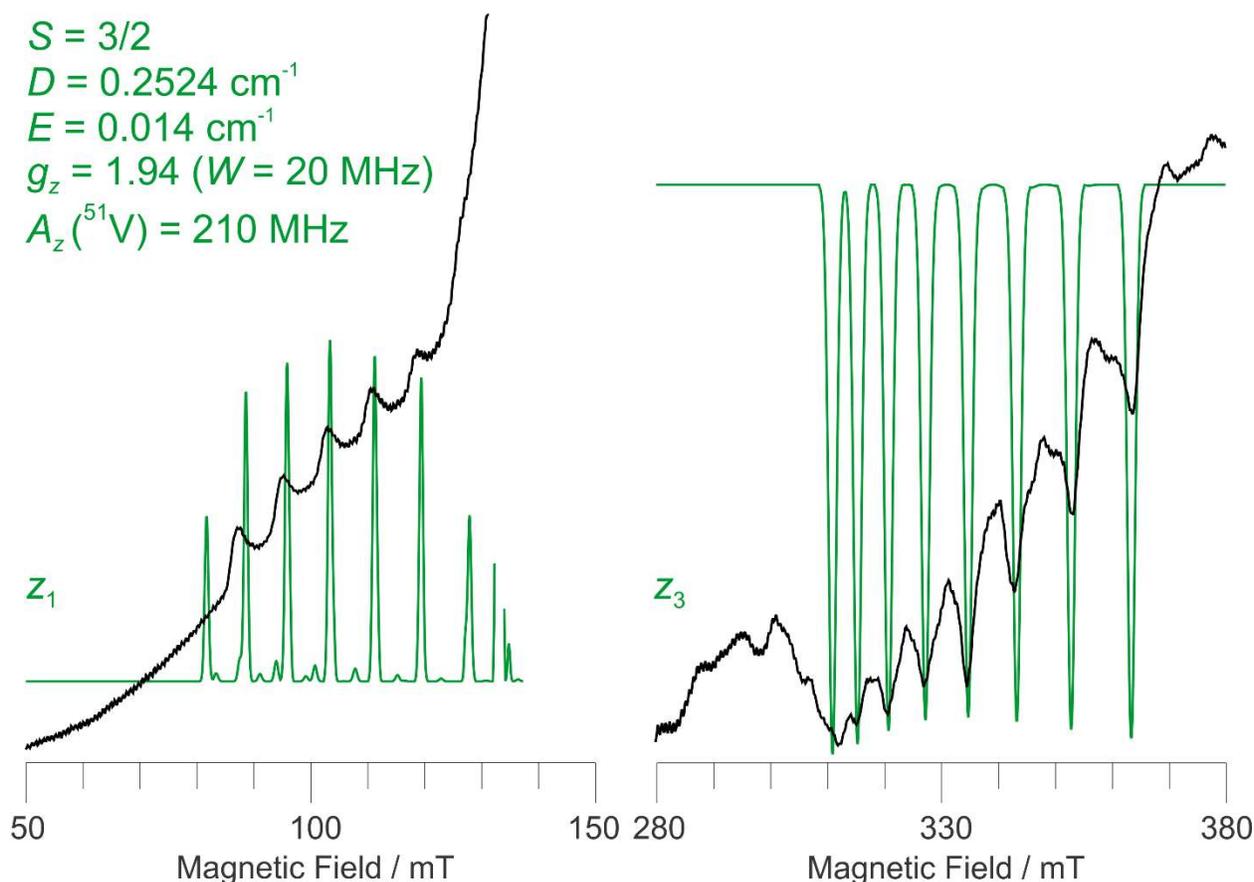
Figure 4. Expansions of X-band EPR spectrum (see Figure 3 for full spectrum and conditions) of *trans*-[VCl$_2$(tmeda)$_2$] (black traces) in the z_1 (left panel) and z_3 (right panel) regions. Simulation (green traces) uses: $S = 3/2$, $D = 0.2524$ cm^{-1}, $E = 0.014$ cm^{-1}, $g_z = 1.94$, A_z(^{51}V) = 210 MHz, Gaussian linewidths of 20 MHz. The narrow simulation linewidth is chosen to make clear the (idealized) ^{51}V ($I = 7/2$, ~100 abundance) hyperfine splitting pattern and not to match the experimental spectrum, which includes underlying broader features from other transitions (*x* and *y*) not simulated.

The X-band EPR spectrum of *trans*-[VCl$_2$(dmpe)$_2$] is shown in Figure 5. Both toluene/DCM and toluene/THF were used with no differences; the figure shows that in the latter solvent. Although the zfs in the dmpe complex is only slightly larger than that in the tmeda complex, the X-band spectra of the two look rather different. Additionally, we speculate that unresolved hyperfine coupling from the four ^{31}P ($I = 1/2$, 100%) donors obscures the ^{51}V hfc in the dmpe complex. ENDOR spectroscopy at 35 GHz was also employed in the hopes of measuring this diphosphine interaction, but was unsuccessful. Tripodal triphosphine ligands bound to

12

paramagnetic Fe[29] and Ni[30] centers have indeed exhibited strong ^{31}P ENDOR signals that were thoroughly analyzed. All these paramagnetic centers, which were both mononuclear[29b, 30-31] and dinuclear,[29a, 29c] have $S = 1/2$ ground states. The present V^{II} complexes with $S = 3/2$ and "medium" zfs (i.e., zfs not so small as to be nearly unobservable, as in $[Cr(NH_3)_6]^{3+}$ and related complexes,[32] but not so large as to be well modeled by an effective $S' = 1/2$, as in trans-$[CrX_2(en)_2]^+$ (X = Cl$^-$, SCN$^-$, HO$^-$)[33]) are thus not well suited for ENDOR investigation due to mixing of m_S levels and complicated electron and nuclear spin relaxation properties. Unresolved ^{51}V hfc also complicates the orientation selection[34] aspect of ENDOR. We were unable to observe any hfc due to ^{14}N ($I = 1$, 99.6%) in the tmeda complex. The reason for this is suggested by QCT as discussed below.

ENDOR signals due to ^{1}H, from the many, weakly (mainly dipolar) coupled hydrogens on the dmpe or tmeda ligand were readily observed across the EPR spectral envelope centered at the corresponding Larmor frequency (e.g., $\nu(^1H) = 53$ MHz for $g = 2.0$ at ~35 GHz). Interestingly, high radiofrequency signals (> 60 MHz; well above the ^{1}H signals) presumably due to ^{51}V ENDOR were observed in both the dmpe and tmeda complexes.

13
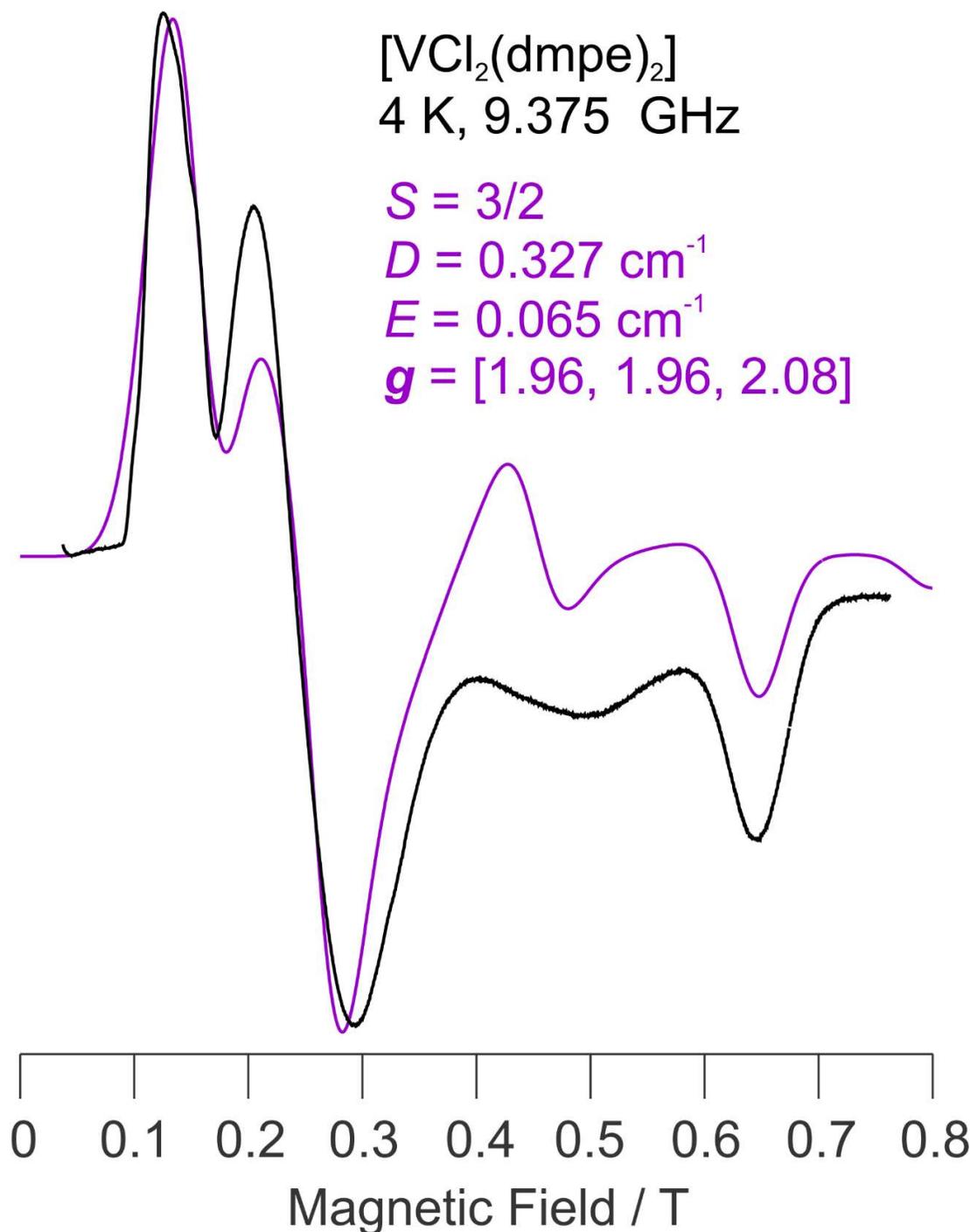
Figure 5. X-band EPR spectrum of *trans*-[VCl₂(dmpe)₂] (black trace) recorded in toluene/THF (1:1 v/v) frozen solution at 4 K and 9.375 GHz with 100 kHz field modulation amplitude of 1 mT; time constant, 320 ms; 90 s scan. Simulation (violet trace) uses: $S = 3/2$, $D = 0.327$ cm^{-1}, $E = 0.065$ cm^{-1}, $\mathbf{g}$ = [1.96, 1.96, 2.08], Gaussian linewidths of 22 mT. No hyperfine coupling from ^{51}V is observed, but unresolved hfc likely contributes to the difficulty in exactly matching the lineshapes. See Figure S8 for Q-band EPR spectra.

14

The X-band EPR spectrum of *trans*-[VCl$_2$(dmpe)$_2$] in toluene frozen solution (77 K) was previously reported by Girolami et al.,[1] and qualitatively resembled that shown here. They were able to reach a field of 1200 mT, which allowed observation of additional fine structure transitions. Their analysis gave $|D| = 0.47$ cm^{-1}, $|E| = 0.041$ cm^{-1} ($E/D = 0.09$), which is slightly different from that found here (see Figure S8, which presents the Q-band spectrum of the dmpe complex with simulations), although we did not use neat toluene. For further comparison, the X-band EPR spectra in frozen solution have been reported (descriptively, without figures, and the solvent is not given, but might be acetonitrile) for *trans*-[VL$_2$(dmpe)$_2$]$^{0,2+}$, where L = MeCN, *t*BuNC, CN$^-$, and NCS$^-$ by Anderson *et al.*[12] For the two complexes with C donor ligands (cyanide and *t*-butylisocyanide), the zfs is small and an upper limit on $|D|$ of 0.01 cm^{-1} was proposed. For *trans*-[V(NCMe)$_2$(dmpe)$_2$][BPh$_4$]$_2$ and *trans*-[V(NCS)$_2$(dmpe)$_2$], the zfs is larger: $0.14 < |D| < 0.16$ cm^{-1} for the acetonitrile complex and $0.3 < |D| < 0.5$ for the thiocyanato complex. Thus, except for the complexes with strong C donors, $|D| = 0.3(2)$ cm^{-1} with little or no E component for the entire *trans*-[V^{II}(X,L)$_2$(R$_2$ECH$_2$CH$_2$ER$_2$)$_2$]$^{0,2+}$ (E = N, P; X = halide, pseudohalide; L = nitrile) series.

HFEPR spectroscopy. As described above, we and others have been able to extract the zfs parameters for *trans*-[V^{II}(X,L)$_2$(R$_2$ECH$_2$CH$_2$ER$_2$)$_2$]$^{0,2+}$ solely from conventional, primarily X-band, EPR spectroscopy. However, a more reliable technique for this purpose is high-frequency and -field EPR (HFEPR),[16, 35] which we therefore applied to to *trans*-[VCl$_2$(tmeda)$_2$] and *trans*-[VCl$_2$(dmpe)$_2$]. Figure 6 presents the HFEPR spectrum of powder *trans*-[VCl$_2$(tmeda)$_2$] recorded at 120 GHz and 20 K. A classic quartet pattern is already obtained at this frequency. The simulation parameters are essentially the same as those used for the conventional EPR spectra (Figures 3 and S6). This spectrum, however, can be simulated equally well with either positive or negative zfs. The sign of zfs can be determined by use of higher frequencies, 244 GHz and 370 GHz, with these shown in Figures S9 and S10, respectively. It is clear from these spectra that D (and by convention, E) is negative. Although only a few frequencies were employed, a two-dimensional field/frequency plot (Figure S11) can be generated using the procedure we have described elsewhere.[35a] . The least-squares fit to the entire dataset yields the following $S = 3/2$ Hamiltonian parameters: $D = -0.257(10)$ cm^{-1}, $E = -0.021(7)$ cm^{-1} ($E/D = 0.082$), $g_x = 1.954(5)$, $g_y = 1.944(6)$, $g_z = 1.961(5)$ ($g_{avg} = 1.953$). Table 3 also lists these spin Hamiltonian parameters.

15
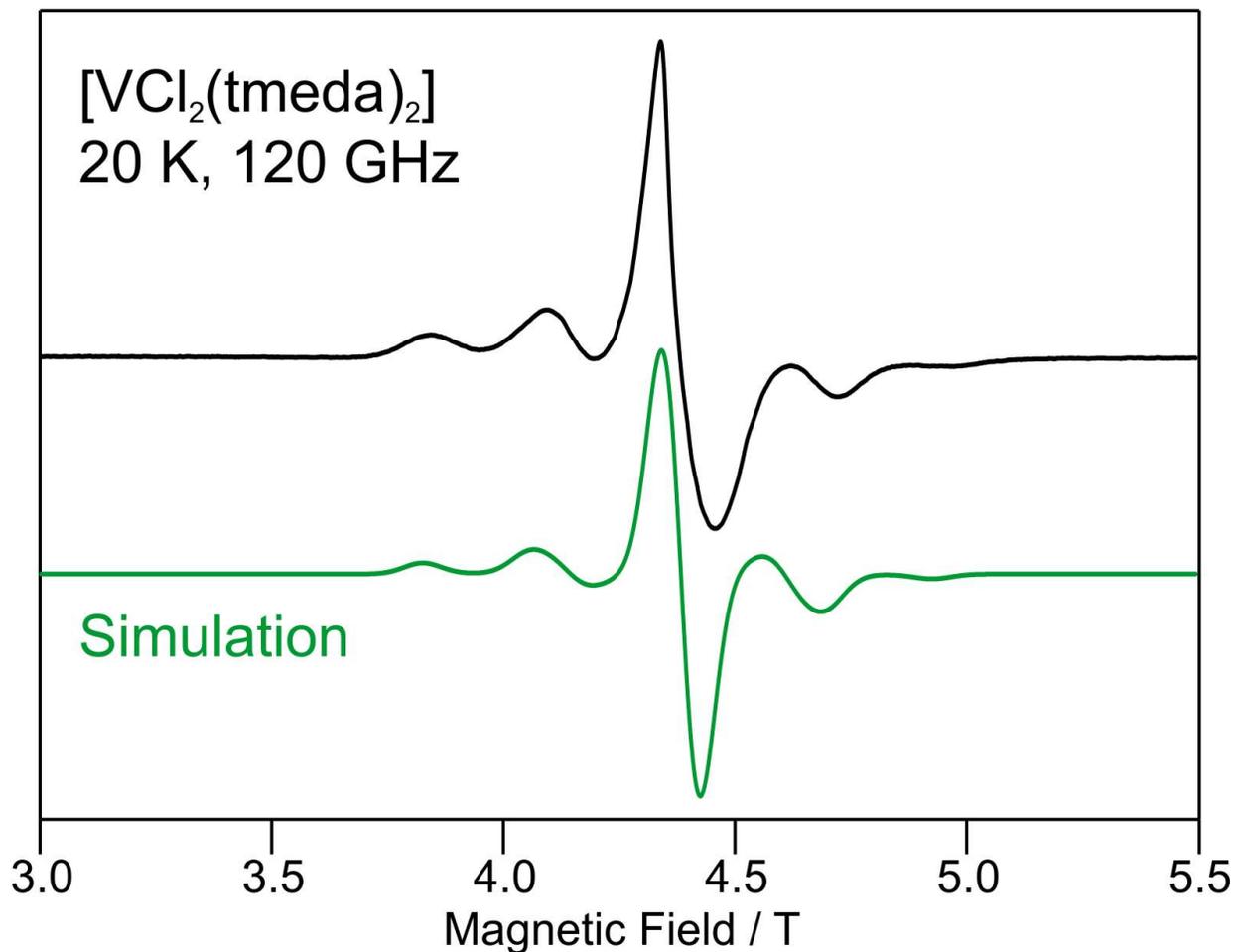
Figure 6. HFEPR spectrum of powder *trans*-[VCl$_2$(tmeda)$_2$] (black trace) recorded at 120 GHz and 20 K. Simulation (green trace) uses: $S = 3/2$, $|D| = 0.2524$ cm^{-1}, $|E| = 0.0140$ cm^{-1}, $g_{iso} = 1.96$, Gaussian linewidths of 20 mT. No hyperfine coupling from ^{51}V is observed in this magnetically non-dilute sample, but unresolved hfc (and slight *g* anisotropy) likely contributes to the difficulty in matching the central lineshape exactly. The simulation matches equally well whether positive or negative zfs parameters are used. Figures S9 and S10 present spectra at higher frequencies that allow the sign of *D* to be determined.

In the case of *trans*-[VCl$_2$(dmpe)$_2$], HFEPR spectra of solid material were uninformative due to the inability to obtain powder pattern spectra, even in fully powdered samples. Fortunately, frozen solution (toluene/DCM, 1:1 v/v) samples gave usable spectra, although a V^{IV} ($S = 1/2$) oxidation product (signal near $g \sim 2.0$) results from handling these highly air-sensitive solutions. In this case, it was again possible to determine the absolute sign of *D*. This is shown in Figure 7,

16

which presents a spectrum recorded at 165.6 GHz and 20 K with simulations for each of *D* positive and negative. It is apparent that *D* > 0, which is also clear from the spectrum recorded at 322 GHz (Figure S12). It is, therefore, likely that a positive *D* value is also the situation for others of the *trans*-[$V^{II}(X,L)_2(R_2PCH_2CH_2PR_2)_2$]$^{0,2+}$ series (except L = C donors).
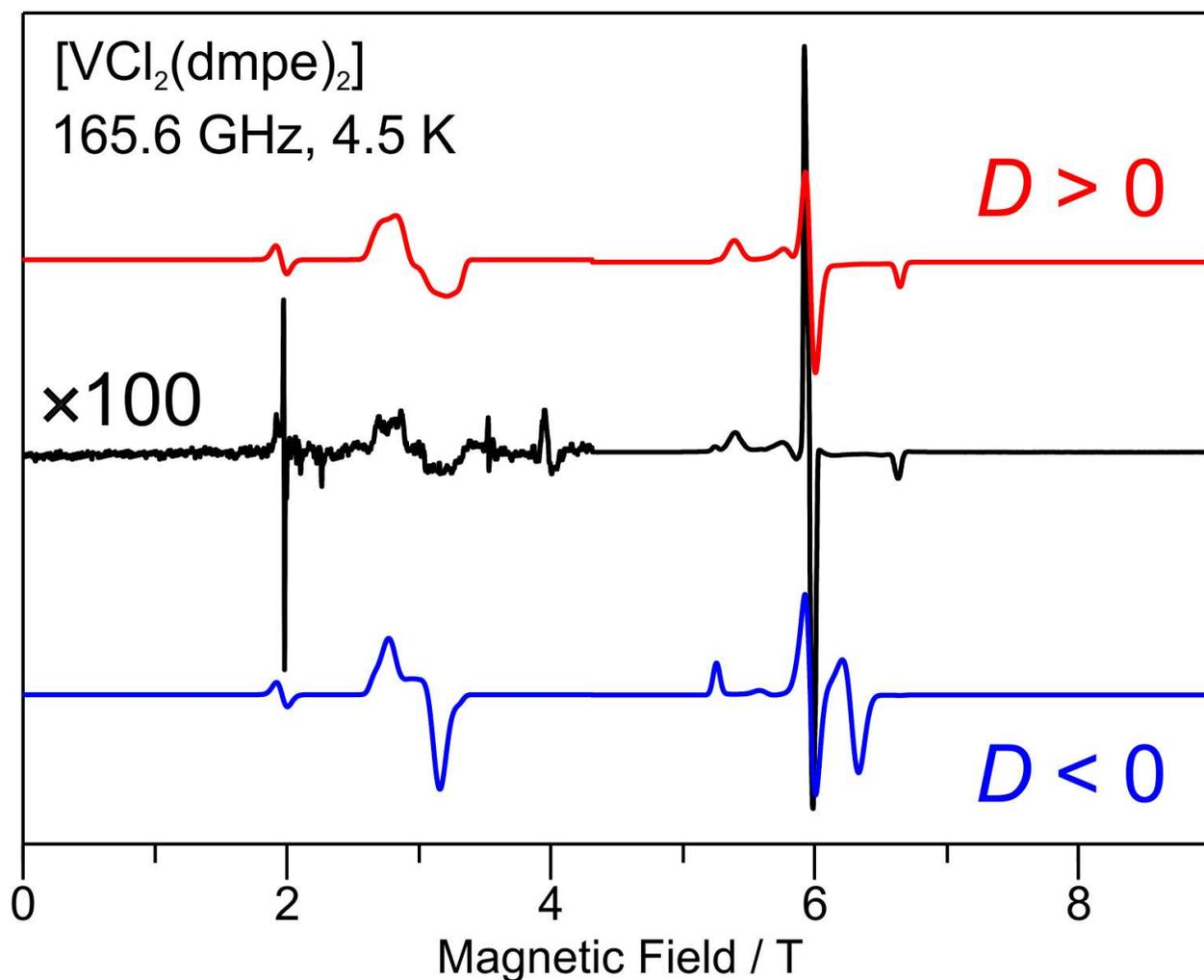
Figure 7. HFEPR spectrum of *trans*-[$VCl_2(dmpe)_2$] in toluene/DCM (1:1 v/v) solution (black trace) recorded at 165.6 GHz and 4.5 K. Simulations use: $S = 3/2$, $|D| = 0.323$ cm^{-1}, $E = 0.0618$ cm^{-1}, **g** = [1.984, 1.989, 1.993]. The blue trace used negative *D*, *E* values; the red trace positive *D*, *E* values. The weak, nominally forbidden transitions below ~4 T are expanded 100× in the experimental trace. It is apparent that the simulation with *D* > 0 better matches experiment.

17

It was possible to record high quality spectra for *trans*-[VCl$_2$(dmpe)$_2$] over a wide range of frequencies and the resulting two-dimensional field/frequency plot is shown in Figure S13. The least-squares fit to the entire dataset yields the following $S = 3/2$ Hamiltonian parameters: $D = +0.323(2)$ cm^{-1}, $E = +0.066(2)$ cm^{-1} ($E/D = 0.20$), $g_x = 1.984(2)$, $g_y = 1.989(3)$, $g_z = 1.993(2)$ ($g_{avg} = 1.989$).

Ligand Field Theory (LFT) – Electronic Transitions and Spin Hamiltonian Parameters. As a background to the case of octahedral d^3 systems, Table S4 presents the energy levels of term symbols for an octahedral d^3 system calculated using a small octahedral splitting and large interelectronic repulsion (Racah) parameters so that all the terms arising from different free-ions are well separated. In the present, highly covalent systems, the terms are interleaved in energy, and their parentage is much more mixed. Table S4 thus provides an idealized situation that is easily understood and, therefore, is helpful for reference in the present and future octahedral d^3 cases.

Octahedral complexes of Cr^{III} are amongst the most widely investigated by classical ligand field theory (LFT) of all coordination complexes,[36] but those of V^{II} less so. Fortunately, LFT has been previously applied to some members of the *trans*-[V^{II}(X,L)$_2$(R$_2$ECH$_2$CH$_2$ER$_2$)$_2$]$^{0,2+}$ series, specifically those with X = Cl and E = N, by Niedwieski et al.[17] These workers used the Ballhausen parameters Dq, Ds, Dt,[37] with which we have used previously, and the δσ and δπ parameters of McClure,[38] which we have not. They followed the earlier work of Baker and Phillips, who had studied the series of analogous, isoelectronic Cr^{III} complexes *trans*-[Cr^{III}(X,L)$_2$(en)$_2$]$^{+,2+,3+}$ (i.e., E = N, R = H) and X or L = H$_2$O, HO$^-$, Cl$^-$, Br$^-$, I$^-$, SCN$^-$.[39] Electronic absorption data for the most relevant of these Cr^{III} complexes are listed in Table S3. The general assignment of electronic absorption bands in these 3d^3 *trans*-[M(X,L)$_2$(R$_2$ECH$_2$CH$_2$ER$_2$)$_2$]$^{0,+,2+,3+}$ complexes is well established now, and is shown qualitatively in Figure 8. In the parent octahedral (O_h) symmetry, the ground state is ^{4}A$_{2g}$(^{4}F) ($t_2^3e^0$ in strong field notation), with the first excited state ^{4}T$_{2g}$(^{4}F) ($t_2^2e^1$), followed by ^{4}T$_{1g}$(^{4}F) ($t_2^1e^2$), and ^{4}T$_{1g}$(^{4}P) ($t_2^2e^1$) at highest energy. The order of the two ^{4}T$_{1g}$ states can vary depending on the ligand-field strength and Racah B parameter, which is also a measure of covalency,[37] and their free-ion parentage is typically very mixed. In the tetragonally distorted complexes under investigation here, the symmetry is lowered to D_{4h} (C_4 axis = z axis = X-M-X bond axis). The ground state is now ^{4}B$_{1g}$, and the ^{4}T$_{2g}$ first excited state

18

splits into $^4B_{2g}$ and $^4E_{g(a)}$, where (*a*) is used to distinguish amongst the other ^4E_g states, as each $^4T_{1g}$ excited state splits into $^4A_{2g}$ and ^4E_g. The latter will also be given subscripts, (*b*) and (*c*) to further distinguish them. The energies of the lower excited states have been determined to first order, and these are provided in Supporting Information. In our analysis of the electronic absorption spectra, we also use the Ballhausen *Dq*, *Ds*, *Dt* parameters,[37] but additionally use the angular overlap model (AOM) as this directly provides information on metal-ligand bonding,[40] and readily allows inclusion of the slight orthorhombic distortion from tetragonal symmetry imposed by the bidentate chelating tmeda and dmpe ligands (see Table S2). Moreover, the AOM allows an improved understanding of π-bonding effects than that given by the Ballhausen *Dq*, *Ds*, *Dt* parameters. We also use least-squares fitting from matrix diagonalization rather than the perturbation theory equation given in Supporting Information and necessarily used in earlier times.[39]
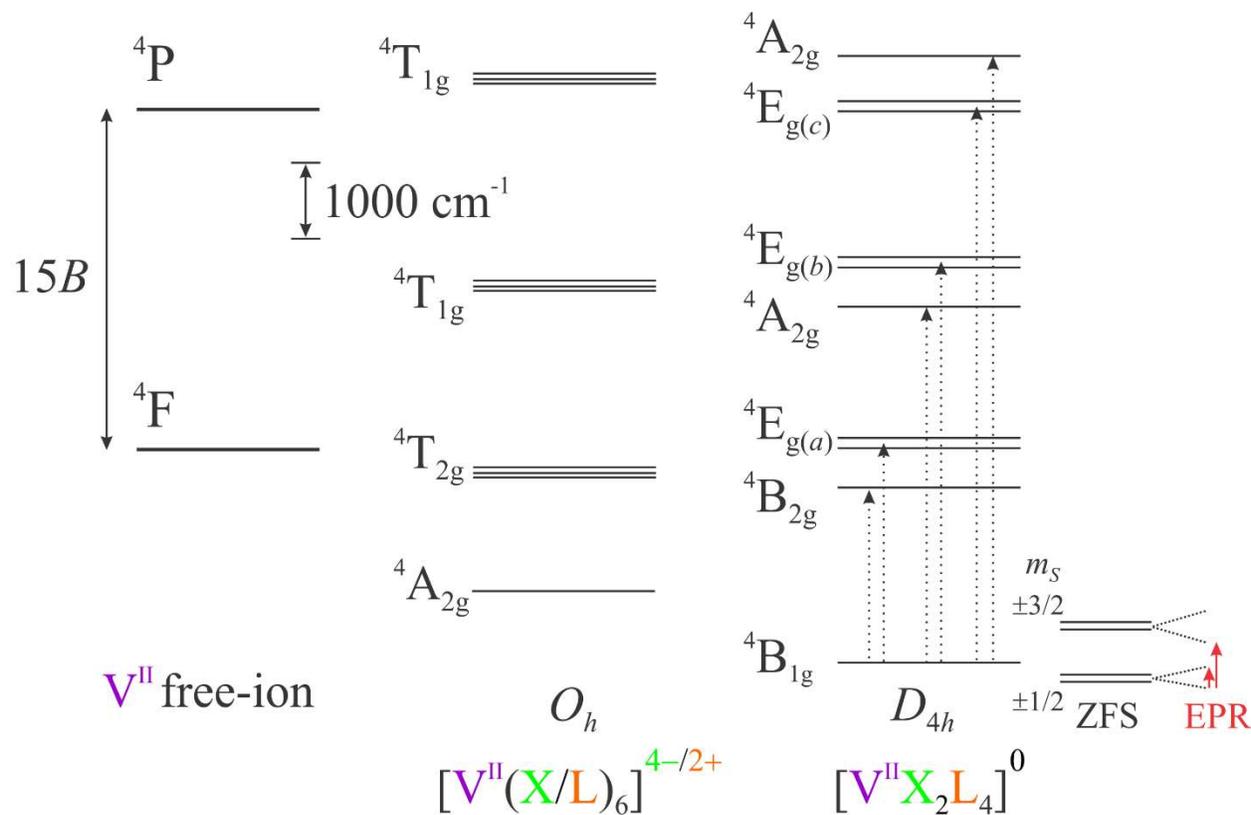
Figure 8. Qualitative LFT diagram for 6-coordinate V^{II} complexes (X = anionic ligand, such as halide, L = neutral ligand, such as ammine or phosphine). The term ordering in D_{4h} symmetry is that proposed for *trans*-[VCl$_2$(RNHCH$_2$CH$_2$NHR)$_2$] using the Ballhausen parameter analysis,[17] but alternate orderings are possible (see text). Spin-allowed electronic transitions are indicated by the dotted vertical arrows. These are all dipole forbidden in true D_{4h} symmetry, but in D_4 symmetry

19

$B_1 \rightarrow B_2$ is z-dipole allowed and $B_1 \rightarrow E$ is x,y-dipole allowed (the idealized symmetry of bischelate, $[V^{II}X_2(L\text{-}L)_2]$, is D_{2h} and that of the real $[V^{II}X_2(R_2ECH_2CH_2ER_2)_2]$ complexes including the effect of the chelate linker is only C_i). The effect of zfs and resulting EPR transitions are qualitatively shown for the electronic ground state term.

Amongst the $trans$-$[MCl_2(R_2ECH_2CH_2ER_2)_2]^{0,+}$ series, the electronic absorption spectrum of $trans$-$[Cr^{III}Cl_2(en)_2]^+$ (Figure 4 in Baker and Phillips[39]) most clearly displays the bands of interest, which are assigned as follows: $^4B_{1g} \rightarrow {}^4E_{g(a)}$ at 17 540 cm^{-1}, $^4B_{1g} \rightarrow {}^4B_{2g}$ at 21 880 cm^{-1}, $^4B_{1g} \rightarrow {}^4E_{g(b)}$ at 25 380 cm^{-1}, and $^4B_{1g} \rightarrow {}^4A_{2g}$ at 27 700 cm^{-1}. In the $trans$-$[VCl_2(RHNCH_2CH_2NHR)_2]$ series, a reversed assignment within each O_h parent was used by Niedwieski et al.[17] (values for tmeda complex): $^4B_{1g} \rightarrow {}^4B_{2g}$ at 11 236 cm^{-1}, $^4B_{1g} \rightarrow {}^4E_{g(a)}$ at 12 346 cm^{-1}, $^4B_{1g} \rightarrow {}^4A_{2g}$ at 16 340 cm^{-1}, and $^4B_{1g} \rightarrow {}^4E_{g(b)}$ at 19 084 cm^{-1}. In the diphosphine complexes, the assignments are less definitive. Holt et al. did not observe the splitting due to tetragonal distortion and thus assigned the three bands seen in diffuse reflectance spectra (in increasing energy) to all three of the O_h parent transitions (values for $[VCl_2(dmpe)_2]$): $^4A_{2g} \rightarrow {}^4T_{2g}$ at 14 200 cm^{-1}, $^4A_{2g} \rightarrow {}^4T_{1g}(F)$ at 19 8000 cm^{-1}, and $^4A_{2g} \rightarrow {}^4T_{1g}(P)$ at 28 000 cm^{-1} (with shoulder at 24 700 cm^{-1}).[10b] Ghosh et al. assigned the lowest energy bands in the $[VX_2(dmpe)_2]$ series to $^4B_{1g} \rightarrow {}^4E_{g(a)}$ and higher energy bands as arising from the O_h parent transition $^4A_{2g} \rightarrow {}^4T_{1g}(F)$.[13]

With this background, we proceed to reanalyze $trans$-$[MX_2(R_2ECH_2CH_2ER_2)_2]^{0,+}$, i.e., only the anionic axial ligand complexes, with the exception of $[Cr(OH_2)_2(en)_2]^{3+}$ for completeness. We first use the Ballhausen model in the interest of reproducing previous work. The results are summarized in Table S5. Use of our least squares fitting method with the reported Ballhausen parameters as a starting point leads to an exact fit (within 0.1 cm^{-1}) for all four observed bands of $[VCl_2(tmeda)_2]$ in THF solvent with some changes in the reported parameters (in cm^{-1}; original values in parentheses): $Dq = 1124$ (1130), $Ds = +637$ (+482), $Dt = -136$ (−120). The other three RNHCH$_2$CH$_2$NHR complexes are also fitted perfectly with only minor adjustment of these parameters (see Table S5). However, the Racah B parameter, which was not determined in the original work,[17] but obtained here from fitting, is very different between the tmeda complex and all three with bis(monoalkylamine) ligands, being 475(15) cm^{-1} in the latter series, but ~700 cm^{-1} in the tmeda complex (see Table S5). The bands for the $trans$-$[Cr(X,L)_2(en)_2]$ complexes are

20

likewise perfectly fitted using refinements of the originally reported parameters,[39] particularly for B, which is less accurately determined using first-order equations (given in Supporting Information) than from the exact calculation employed here.

Concerning the diphosphine complexes, no quantitative LFT analysis has hitherto been done, and while a large number of complexes of general formula *trans*-[VX$_2$(R$_2$PCH$_2$CH$_2$PR$_2$)$_2$] have been studied, their electronic absorption spectra are less clear-cut than in the diamine complexes, whether V^{II} or Cr^{III}. We begin by using the Ballhausen parameters. The simplest assignment is that the NIR band (~700 – 800 nm; see Table S3) corresponds to $^4B_{1g} \rightarrow [^4B_{2g},$ $^4E_{g(a)}(^4T_{2g})]$ (given in D_{4h}, with O_h parent), which directly gives Dq (disregarding the axial distortion) so that B can be readily determined from the visible band (~500 – 600 nm), which corresponds to $^4B_{1g} \rightarrow [^4A_{2g}, ^4E_{g(b)}(^4T_{1g}(^4F)]$. The diffuse reflectance data of Holt et al.,[10b] thus give B = 557.1, 472.5, and 262.4 cm^{-1}, with Dq = 1420.4, 1270.6, and 1200.5 cm^{-1} for the closely related chlorido dmpe, depe, and dppe complexes, respectively. The calculated energy of the blue to UV band (< ~450 nm) is higher than that observed, but this band may not be a true d-d transition, having MLCT character. This method was also applied to the *trans*-[VX$_2$(R$_2$PCH$_2$CH$_2$PR$_2$)$_2$] (X = Br$^-$, I$^-$, CF$_3$SO$_3^-$, BH$_4^-$; R = Me, Et, Ph) complexes with the results summarized in Table S5. Only for X = CH$_3^-$ is it impossible to fit the data with this model, as there is no band in the red/NIR region (see Table S3). The resulting values for Racah B in this model are reasonable, ranging from ~35 – 75% of the free-ion value. However, for the heavier halides (Br and I), the B fit value is relatively large, which may arise from the effect of covalency with these heavy atoms. The unusual effect of axial diiodido coordination on the electronic structure of a Mn^{III} complex structurally similar to *trans*-[VX$_2$(R$_2$PCH$_2$CH$_2$PR$_2$)$_2$] was pointed out by Mossin et al.[41]

In selected complexes, most importantly here in *trans*-[VCl$_2$(dmpe)$_2$], it is possible to use the larger number of reported bands to estimate a tetragonal distortion using the Ballhausen Ds, Dt parameters as described above for the bisdiamino complexes. These results are also given in Table S5 and show that the transitions can be successfully modeled simply with the addition of tetragonal splitting given by Dt, although the inclusion of Ds can also be helpful. The effect of these parameters is shown in equations S1 and S2 (Supporting Information).

Given this ability to use LFT with the less intuitive Ballhausen parameters, we next apply the more chemically useful AOM.[40] We begin with the more tractable diamine complexes. In this

21

case, there are only three bonding parameters: $\varepsilon_\sigma(X)$, $\varepsilon_\sigma(N)$, and $\varepsilon_\pi(X)$ assuming that both halide donors and all four amine N donors are each equivalent and that the halide is a cylindrical π-donor and the amines only σ-donors. We also use ideal D_{4h} symmetry, disregarding the bite angle of the diamine ligands. The relationship $\Delta_o = 10Dq = 3\varepsilon_\sigma$ allows an initial guess as to the average σ-bonding in the complex using the Dq values determined above. The B value can also be initially set from the above fits. All four diamine complexes can be successfully fitted by the AOM with reasonable parameters with *trans*-[VCl$_2$(tmeda)$_2$] perfectly modelled. However, as shown in Tables S6 and S7, the assignments are different from those obtained using the Ballhausen parameters. Regardless of the fit process, the optimal fit occurs when the band assignments are ($^4B_{1g} \rightarrow$ quartet excited state, in increasing energy): $^4E_{g(a)}$, $^4B_{2g}$ (from $^4T_{2g}(F)$) and $^4E_{g(b)}$, $^4A_{2g}$ (from $^4T_{1g}(F)$), with $^4A_{2g}$, $^4E_{g(c)}$ ($^4T_{1g}(P)$) too high in energy to be observed independently of CT bands. Thus, the ordering of the ^{4}(A, B) and ^{4}E terms within each ^{4}T term are opposite of that proposed earlier and reproduced here (Table S4), so that the assignment for bands from $^4T_{2g}(F)$ proposed[39, 42] for Cr^{III} apply here as well. For the three *trans*-[VCl$_2$(RNHCH$_2$CH$_2$NHR)$_2$] complexes, the situation is more equivocal. The dieda complex is likewise perfectly fitted using the same assignment as for the tmeda complex, as is the dmeda[27] complex, but the latter can also be fitted adequately using the original assignment for the lower energy band (i.e., $^4B_{1g} \rightarrow {}^4B_{2g}$, $^4E_{g(a)}$), while the deeda[27] complex can be fitted adequately using only this assignment. In all cases, however, the higher energy (i.e., visible) band assignment must be $^4B_{1g} \rightarrow {}^4E_{g(b)}$, $^4A_{2g}$. The fit parameters are similar among the diamine complexes, with the deeda complex being the most different, as expected from its different assignment (and poorer fit). The dieda[27] and dmeda fit values are overall relatively close with $B \approx 400$ cm^{-1} (~600 cm^{-1} for [VCl$_2$(tmeda)$_2$]) and all three have ε_σ(Cl) = 5300 $\pm$ 500 cm^{-1}, ε_π(Cl) = 1200 $\pm$ 200 cm^{-1}, and ε_σ(N) = 4500 $\pm$ 500 cm^{-1} (specific values are in Table S6). These values are reasonable in the context of those reported for *trans*-[CrCl$_2$(en)$_2$]$^+$,[42-43] with ε_σ(Cl) and ε_π(Cl) being similar and ε_σ(N) being somewhat smaller for V^{II} as a consequence of its lower charge compared to Cr^{III}.

We next turn to the diphosphine complexes that are more challenging to address because their optical spectra are less informative and there is now an additional variable, ε_π(P), since phosphines can be π-acceptors. However, the low t_{2g} occupancy of 3d^3 V^{II} as opposed to say, 3d^6

22

Co^{III}, makes this effect presumably the least consequential of the four bonding parameters. Only a few of the reported diphosphino complexes warrant the AOM analysis, namely those for which at least one tetragonal splitting can be discerned (see Tables S3 and S5): *trans*- [VCl$_2$(dmpe)$_2$], *trans*-[VBr$_2$(depe)$_2$], *trans*-[VI$_2$(dmpe)$_2$], and *trans*-[V(O$_3$SCF$_3$)$_2$(tmeda)$_2$]. Even in these cases, it is difficult to determine definitively the relative order of terms in D_{4h} within the $^4T_{(1,2)g}$ parent terms. All possible combinations were explored, and the viable results were summarized in Tables S6 and S7. As noted above, there are three data sets for *trans*-[VCl$_2$(dmpe)$_2$] and each gives a distinct set of fit parameters using the AOM (Table S6). Although it was possible to fit our experimental data moderately well using only σ-donation, this was not the case for the other two data sets. However, inclusion of significant π-donation by Cl$^-$ led to perfect fits for all three data sets (Table S7). Inclusion of π-acceptance by P had only a modest effect and might be considered overparameterization, but did lead to ε$_σ$(Cl, P) and particularly ε$_π$(Cl) being more satisfying in the context of other, Cr^{III,II} complexes.[26, 42-43] Comparing the results for the three data sets, the values for ε$_σ$(P) are relatively consistent: ε$_σ$(P) ≈ 4600(100) cm^{-1} with π-acceptance and ε$_σ$(P) ≈ 4800(200) cm^{-1} without. However, there is much greater variation in the values for ε$_σ$(Cl) and ε$_π$(Cl) (when included), which we speculate may be a manifestation of the interaction between the axial chlorido ligands and their environment (relatively inert toluene solvent, H-bonding DCM solvent, and whatever intermolecular interactions are present in the solid-state). In contrast the P donors are sterically protected in the dmpe ligands. We can also make a qualitative comparison of the bonding parameters for Cl between the tmeda and dmpe complexes in relation to their V-Cl bond distances. For *trans*-[VCl$_2$(dpme)$_2$], ε$_σ$(Cl) ≈ 6600 cm^{-1} (average of the various fitting models; Table S6), while for *trans*-[VCl$_2$(tmeda)$_2$], ε$_σ$(Cl) ≈ 5400 cm^{-1} (ε$_π$(Cl) is similar between the two). The greater ε$_σ$(Cl) in the dmpe complex is consistent with its shorter bond distance (by ~0.046 Å).

The fitting process disregards the doublet excited states (i.e., spin forbidden transitions) by use of a large Racah *C* value. Inclusion of a realistic *C* value, namely that with roughly the same reduction from its free-ion value as empirically determined for *B*, provides information on the doublet excited states, which can also contribute to zfs. For illustration, we present in Table S8 the energy level results calculated using the program Ligfield[23] for *trans*-[VCl$_2$(tmeda)$_2$] using the previously reported data[17] and for *trans*-[VCl$_2$(dmpe)$_2$] using our electronic absorption data.

23

What is notable here is that, in contrast to the "pedagogical" case (Table S4), there are calculated to be numerous low-lying doublet excited states. For example, in *trans*-[VCl$_2$(tmeda)$_2$], there are ^2E_g and $^2B_{1g}$ states lying just below (at 10 716 and 11 077 cm^{-1}, respectively) the $^4E_{g(a)}$ state that is assigned to the NIR band (Table S7) and a $^2A_{1g}$ state that is at essentially the same energy (11 278 cm^{-1}). The O_h parentage of these doublets is difficult to determine and they all have mixed ^2H, ^2G, and ^2P free-ion parentage. In *trans*-[VCl$_2$(dmpe)$_2$], there are several doublet states at low energy (~9 800 – 11 100 cm^{-1}) that would give rise to spin-flip transitions, but none is observed. There are no doublet excited states nearby the quartet $^4B_{2g}$ and $^4E_{g(a)}$ states from $^4T_{2g}$; however, there are $^2A_{1g}$ and ^2E_g states bracketing the $^4A_{2g}(^4T_{1g}(F))$ excited state (see Table S8B). There may thus be some nominally spin-forbidden contribution to the observed bands. The QCT section also discusses the doublet excited states.

For the other complexes (i.e., X ≠ Cl$^-$) there is no need to include π-bonding from either the diphosphine ligands or axial anionic ligands (Br$^-$, I$^-$, and also CF$_3$SO$_3^-$). This type of bonding could be forced, for example, by requiring a selected ratio of $\varepsilon_\pi(X)$ to $\varepsilon_\sigma(X)$, but that would be totally arbitrary. Nevertheless, the results for these three complexes are consistent with those for *trans*-[VCl$_2$(dmpe)$_2$] in that $\varepsilon_\sigma(P) \approx 4300(500)$ cm^{-1} and the B value is essentially the same among three halide complexes ($B \approx 600(50)$ cm^{-1}). That for the CF$_3$SO$_3^-$ is in line with those for several of the diamine complexes.

With the above description of the electronic structures of [VCl$_2$(tmeda)$_2$] and [VCl$_2$(dmpe)$_2$], we can then include spin-orbit coupling (SOC) to see if the spin Hamiltonian parameters obtained from paramagnetic resonance can be reproduced. Note that the D_{4h} model employed above for analyzing optical spectra perforce yields only axial spin Hamiltonian parameters ($x \equiv y$, so $E \equiv 0$, $g_x = g_y \equiv g_\perp$); D_{2h} symmetry is more realistic for these bischelate complexes and is presumably the basis for the rhombic zfs observed (Table 3). The QCT studies described below are thus more realistic, but LFT can still be instructive. For *trans*-[VCl$_2$(dmpe)$_2$], using the fit to our electronic absorption data, inclusion of the single-electron SOC constant $\zeta = 125$ cm^{-1} and Racah $C = 2150$ cm^{-1} (each 74% of the free-ion value, as found for B) gives a splitting between the $m_S = \pm 3/2$ ground state and $m_S = \pm 1/2$ ground state of only 0.01 cm^{-1} so that $D = -0.005$ cm^{-1}. The inclusion of an applied field of 300 mT allows the calculation of $g_\perp' \approx g_\parallel' = 1.98$. Results using the data of Ghosh et al.[13] are similar in magnitude of D, but with a positive

24

sign, although the tiny magnitude in both cases makes the sign relatively inconsequential. However, the use of fit values to the diffuse reflectance data,[10b] gives $D = -0.04$ cm^{-1} and while $g_\parallel' = 1.98$, $g_\perp' \approx 4.0$, namely a situation closer to what is observed at X-band (Figure 5). In the case of *trans*-[VCl$_2$(tmeda)$_2$], the situation is similar in that the calculated D value is very small and, in this case, positive: $D \approx 0.02$ cm^{-1}, opposite from experiment, with the g values ~1.97. The zfs calculated here by LFT is that only from SOC (D_{SOC}), with spin-spin coupling (SSC) not included. Even though the SSC contribution is typically small (see below), the LFT model employed here, while adequately modeling the optical spectra, is lacking a full picture of electronic structure. QCT, as described in the following section, helps remedy this deficiency.

Quantum Chemical Theory – Electronic Structure and Ligand-field Excited States. To complement and extend the above, classical LFT approach, we performed both DFT and *ab initio* QCT computations to examine the zfs and excited states of *trans*-[VCl$_2$(R$_2$ECH$_2$CH$_2$ER$_2$)$_2$]. In this analysis, we use term symbols from the D_{2h} point group.

DFT calculations for *trans*-[VCl$_2$(tmeda)$_2$] and *trans*-[VCl$_2$(dmpe)$_2$] allow us to compare and contrast the V^{II} 3d orbital splitting pattern and MO compositions for these complexes (Figure 9 and Table 1). In each complex, the splitting of the V^{II} 3d-based MOs follows that expected for a six-coordinate complex with a slight tetragonal distortion. The a$_g$(d$_{xy}$) MO is the lowest-energy V^{II} 3d MO. This MO is essentially nonbonding in *trans*-[VCl$_2$(tmeda)$_2$], with only minor contributions from ligand orbitals. This situation is expected, as the equatorial N donors for this complex do not have orbitals suitable for π-interactions with the metal center, as noted above in the LFT analysis. Although the equatorial P donors for *trans*-[VCl$_2$(dmpe)$_2$] can participate in π-interactions with the V^{II} center, the DFT calculations predict these interactions to be modest (<7% P character for both the α- and β-spin a$_g$(d$_{xy}$) MOs), again in agreement with LFT (Table S6). The modest π-contributions from the dmpe ligands contrasts with that observed for the corresponding Cr^{II} complex *trans*-[CrCl$_2$(dmpe)$_2$].[26] In that case, the α- and β-spin a$_g$(d$_{xy}$) MOs contained 14 and 21% P character, respectively.
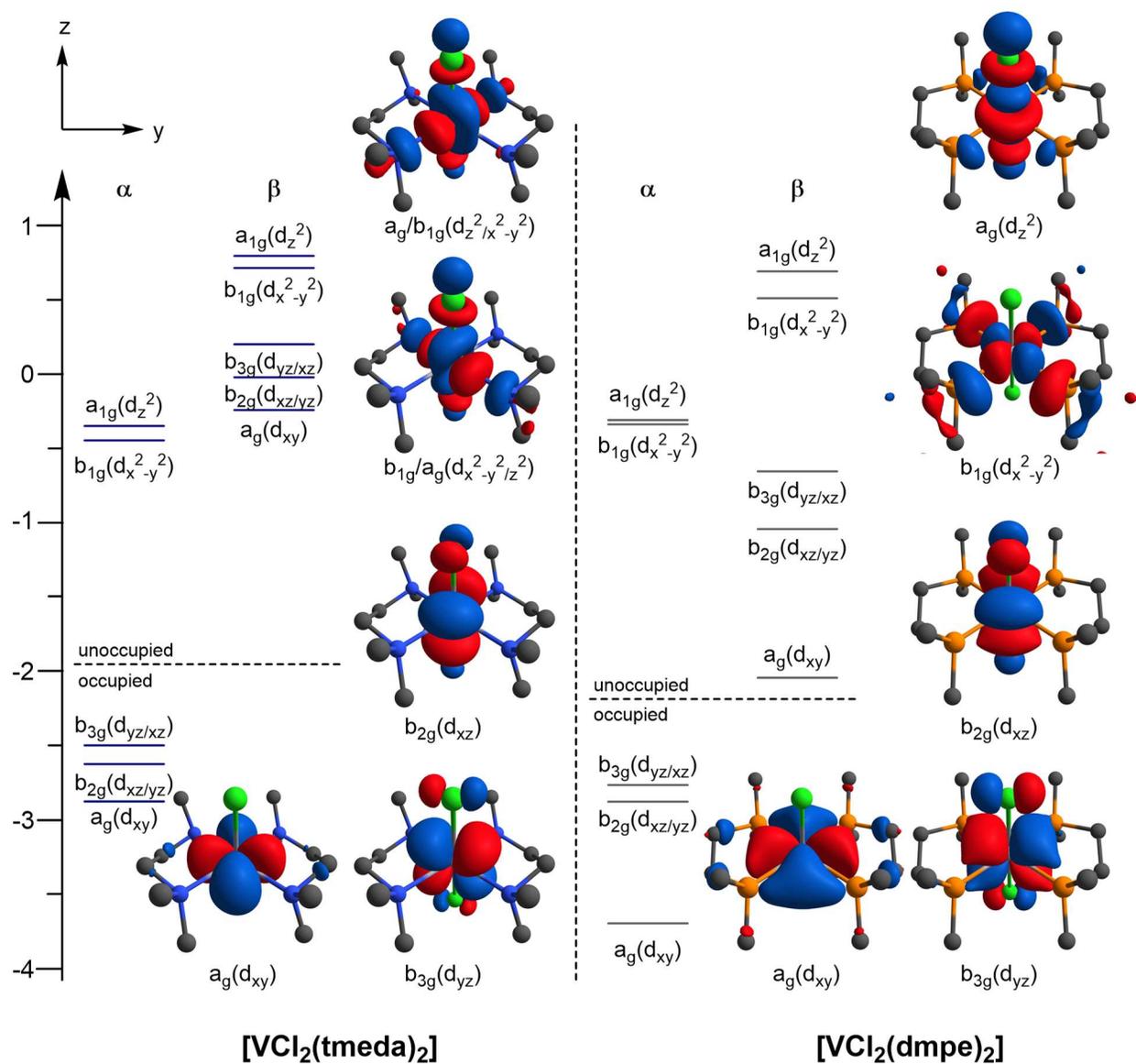
Figure 8. Frontier orbital energy level diagrams of Kohn-Sham MOs and surface contour plots of quasi-restricted MOs for *trans*-[VCl$_2$(tmeda)$_2$] (left) and *trans*-[VCl$_2$(dmpe)$_2$] (right) based on spin unrestricted DFT calculations.

26

Table 1. Molecular Orbital Labels (in D_{2h}), Energies (eV), and Percent Compositions Based on Spin Unrestricted DFT Computations for *trans*-[VCl$_2$(tmeda)$_2$] and *trans*-[VCl$_2$(dmpe)$_2$].

MO	MO label	Occupancy	Energy	V 3d	Cl 3p + 3s	N or P p + s
trans-[VCl$_2$(tmeda)$_2$]						
93α	$a_g(d_{xy})$	1.0	-2.8730	92.9	0.0	0.4
94α	$b_{3g}(d_{xz})$	1.0	-2.6248	86.4	8.4	0.4
95α	$b_{2g}(d_{yz})$	1.0	-2.5169	87.8	8.0	0.2
96α	$b_{1g}/a_g(d_{x^2-y^2/z^2})$	0.0	-0.4471	77.6	6.2	7.6
97α	$a_g/b_{1g}(d_{z^2/x^2-y^2})$	0.0	-0.3662	76.5	5.2	9.2
93β	$a_g(d_{xy})$	0.0	-0.2499	76.4	0.0	0.0
94β	$b_{3g}(d_{xz})$	0.0	-0.0307	79.6	3.6	1.8
95β	$b_{2g}(d_{yz})$	0.0	0.1924	82.0	4.2	0.8
98β	$b_{1g}/a_g(d_{x^2-y^2/z^2})$	0.0	0.6899	74.0	4.4	4.8
99β	$a_g/b_{1g}(d_{z^2/x^2-y^2})$	0.0	0.7855	74.6	3.6	6.4
trans-[VCl$_2$(dmpe)$_2$]						
109α	$a_g(d_{xy})$	1.0	-3.6872	75.9	0.0	1.8
110α	$b_{3g}(d_{xz})$	1.0	-2.9096	73.6	14.8	1.2
111α	$b_{2g}(d_{yz})$	1.0	-2.7643	78.2	13.4	0.6
112α	$b_{1g}(d_{x^2-y^2})$	0.0	-0.3310	76.0	0.0	18.4
113α	$a_g(d_{z^2})$	0.0	-0.3243	66.0	13.6	5.2
109β	$a_g(d_{xy})$	0.0	-2.0483	55.5	0.0	6.8
110β	$b_{3g}(d_{xz})$	0.0	-1.0528	57.9	9.0	6.2
111β	$b_{2g}(d_{yz})$	0.0	-0.6589	67.7	7.8	4.2
114β	$b_{1g}(d_{x^2-y^2})$	0.0	0.4805	58.6	0.0	14.0
116β	$a_g(d_{z^2})$	0.0	0.6660	60.0	8.4	6.4

The V^{II} $b_{3g}(d_{yz})$ and $b_{2g}(d_{xz})$ MOs of *trans*-[VCl$_2$(tmeda)$_2$] and *trans*-[VCl$_2$(dmpe)$_2$] lie above the $a_g(d_{xy})$ MO and are involved in V-Cl π-antibonding interactions (Figure 8 and Table 1). The splitting between the $a_g(d_{xy})$ and $b_{3g}(d_{yz})/b_{2g}(d_{xz})$ MOs of *trans*-[VCl$_2$(tmeda)$_2$] is much smaller than that of *trans*-[VCl$_2$(dmpe)$_2$] (~0.3 eV or ~2500 cm^{-1} versus ~1 eV or ~8000 cm^{-1}, respectively). The larger splitting for *trans*-[VCl$_2$(dmpe)$_2$] is caused by greater V-Cl π-covalency (Table 1). Previous calculations for *trans*-[CrCl$_2$(dmpe)$_2$] and *trans*-[TiCl$_2$(tmeda)$_2$] revealed substantially more Cl π-covalency in the former complex (~18% versus ~4 – 8% Cl admixture in

27

the metal b$_{3g}$(d$_{yz}$) and b$_{2g}$(d$_{xz}$) MOs).[8, 26] Thus, complexes with the dmpe ligands have larger metal-chloride covalency even with a change in the metal center.

While the splitting between the a$_g$(d$_{xy}$) and b$_{3g}$(d$_{yz}$)/b$_{2g}$(d$_{xz}$) MOs are different between the *trans*-[VCl$_2$(tmeda)$_2$] and *trans*-[VCl$_2$(dmpe)$_2$] complexes, the splitting within the b$_{3g}$(d$_{yz}$) and b$_{2g}$(d$_{xz}$) MOs is comparable (Table A). For *trans*-[VCl$_2$(tmeda)$_2$], the calculated splitting of the b$_{3g}$(d$_{yz}$) and b$_{2g}$(d$_{xz}$) MOs (0.22 eV or 1800 cm^{-1} for the β spin MOs) is smaller than that observed for the corresponding Ti^{II} complex *trans*-[TiCl$_2$(tmeda)$_2$] (0.52 eV or 4180 cm^{-1} for the β spin MOs).[8] The b$_{3g}$(d$_{yz}$)-b$_{2g}$(d$_{xz}$) splitting in *trans*-[VCl$_2$(dmpe)$_2$] is comparable to that of the Cr^{II} complex *trans*-[CrCl$_2$(dmpe)$_2$] (~0.2 eV).[26]

The DFT calculations for *trans*-[VCl$_2$(tmeda)$_2$] predict the b$_{1g}$(d$_{x^2-y^2}$) and a$_g$(d$_{z^2}$) MOs to be essentially isoenergetic, each lying ~1 – 2.5 eV above the a$_g$(d$_{xy}$) MO (with the larger splitting for the α MOs; see Figure 8). Both MOs show σ-antibonding interactions with the Cl and N donors, and surface contour plots of these MOs reveal strong mixing of the canonical b$_{1g}$(d$_{x^2-y^2}$) and a$_g$(d$_{z^2}$) MOs (Figure 8). In contrast, the b$_{1g}$(d$_{x^2-y^2}$) and a$_g$(d$_{z^2}$) MOs for *trans*-[VCl$_2$(dmpe)$_2$] show a larger destabilization (~2.5 – 3.4 eV) relative to the a$_g$(d$_{xy}$) MO than in complex *trans*-[VCl$_2$(tmeda)$_2$]. These MOs have more covalent mixing with the Cl and P donors and retain their canonical shapes (Figure 8).

Overall, the DFT calculations indicate that important differences between the 3d MOs of the *trans*-[VCl$_2$(tmeda)$_2$] and *trans*-[VCl$_2$(dmpe)$_2$] complexes can be linked to more covalent interactions in the latter complex. First, the increased V-Cl π-covalency in *trans*-[VCl$_2$(dmpe)$_2$] leads to a larger splitting between the a$_g$(d$_{xy}$) and b$_{3g}$(d$_{yz}$)/b$_{2g}$(d$_{xz}$) MOs. Second, the larger σ-covalency of *trans*-[VCl$_2$(dmpe)$_2$] with both the Cl and P ligands leads to a larger gap between the a$_g$(d$_{xy}$) and b$_{1g}$(d$_{x^2-y^2}$)/a$_g$(d$_{z^2}$) MOs.

To understand how these differences in 3d energies and composition influence the ligand-field excited states of *trans*-[VCl$_2$(tmeda)$_2$] and *trans*-[VCl$_2$(dmpe)$_2$], we used both TD-DFT and CASCF/NEVPT2 methods to calculate excited states of these V^{II} centers. The TD-DFT method only yields one-electron quartet excited states, while the CASSCF/NEVPT2 method yields both quartet and doublet exited states, including one- and two-electron excitations. We begin our discussion with the CASSCF/NEVPT2 states, as this method offers the most complete description of the ligand-field states.

28

The CASSCF/NEVPT2 states for *trans*-[VCl$_2$(tmeda)$_2$] and *trans*-[VCl$_2$(dmpe)$_2$] are shown in Figure 9 and Table 2, where we include the parentage of these states from the O_h point group. For a d^3 metal complex in O_h symmetry, the electronic ground is the orbitally non-degenerate $^4A_{2g}$ state, and there are three quartet excited states ($^4T_{2g}$, $^4T_{1g}$(F), and $^4T_{1g}$(P)). A descent in symmetry from O_h to D_{2h} causes each ^4T excited state to split into three components (Figure 9). A larger number of doublet excited states are also predicted for a d^3 metal ion in O_h symmetry, the lowest-lying of which are the ^2E_g, $^2T_{1g}$, and $^2T_{2g}$ states (Table 2). Depending on the precise combination of ligand field strength (10Dq) and metal ion electron-electron repulsion (Racah *B* parameter), the lowest-energy quartet and doublet states will interleave one another (unlike in the simplified case shown in Table S4).
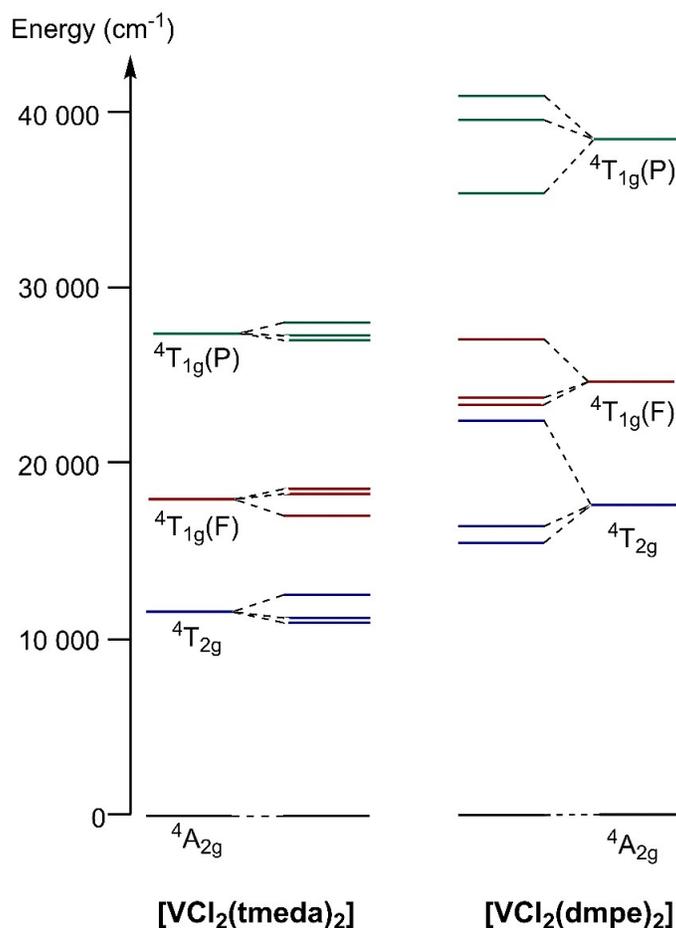
Figure 9. Ligand-field ground and excited states for *trans*-[VCl$_2$(tmeda)$_2$] and *trans*-[VCl$_2$(dmpe)$_2$] from CASSCF/NEVPT2 calculations. States are shown as deriving from their O_h terms (edges).

29

Table 2. Energies (cm^{-1}) of Ligand-Field States of *trans*-[VCl$_2$(tmeda)$_2$] and *trans*-[VCl$_2$(dmpe)$_2$] from CASSCF/NEVPT2 Calculations.

O_h parent state	D_{2h} state [a]	*trans*-[VCl$_2$(tmeda)$_2$]		*trans*-[VCl$_2$(dmpe)$_2$]	
		TD-DFT	NEVPT2	TD-DFT	NEVPT2
$^4A_{2g}$	$^4B_{1g}$		0		0
^2E_g	$^2B_{1g}$		13 423		10 858
	^2A_g		13 514		11 726
$^2T_{1g}$	$^2B_{3g}$		13 662		7 757
	$^2B_{1g}$		14 395		12 735
	$^2B_{2g}$		14 455		8 732
$^2T_{2g}$	$^2B_{3g}$		19 366		21 691
	^2A_g		19 720		19 048
	$^2B_{2g}$		19 788		19 982
$^4T_{2g}$	$^4B_{2g}$ [a]	13 439	10 890	*17 439* [b]	15 487
	$^4B_{3g}$ [a]	13 816	11 037	16 720	16 374
	^4A_g	15 407	12 438	*23 262*	22 415
$^4T_{1g}$(F)	$^4B_{2g}$	18 049	16 932	20 889	23 308
	$^4B_{1g}$	*20 216* [b]	18 176	*26 498*	*27 087* [b]
	$^4B_{3g}$	19 106	18 544	21 028	23 751
$^2A_{1g}$	^2A_g		22 253		21 122
$^2\Gamma$	$^2B_{2g}$		24 698		27 313
	$^2B_{3g}$		24 878		26 993
	$^2B_{2g}$		25 382		28 795
	$^2B_{3g}$		25 410		27 403
	^2A_g		26 295		33 323
	^2A_g		26 662		33 978
	^2A_g		26 845		*ND* [c]
	$^2B_{1g}$		27 696		34 356
$^4T_{1g}$(P)	$^2B_{3g}$		26 964		*40 968*
	$^2B_{1g}$		27 051		*35 361*
	$^2B_{2g}$		28 237		39 469

[a] The term symbols for the ground and excited states were determined from the electronic configurations of the CASSCF calculations.
[b] States that change their energetic ordering relative to CASSCF/NEVPT2 results for *trans*-[VCl$_2$(tmeda)$_2$] are indicated in *italics*.
[c] We were unable to identify this excited state.

For the *trans*-[VCl$_2$(tmeda)$_2$] and *trans*-[VCl$_2$(dmpe)$_2$] complexes, the CASSCF/NEVPT2 calculations predict a $^4B_{1g}$ ground state (derived from the parent $^4A_{2g}$ state), arising from a $(a_g)^1(b_{2g})^1(b_{3g})^1(b_{1g})^0(a_g)^0$ configuration. For *trans*-[VCl$_2$(tmeda)$_2$], the quartet excited states are predicted in clusters derived from the $^4T_{2g}$, $^4T_{1g}$(F), and $^4T_{1g}$(P) parent states near ~11 500 (~870

30

nm), 17 900 (~560 nm), and 27 500 cm^{-1} (364 nm), respectively. The positions of these transitions are in reasonable agreement with the experimental electronic absorption bands at 10 600 cm^{-1} (~940 nm), 16 700 cm^{-1} (~600 nm), and 25 000 cm^{-1} (~400 nm). The individual states derived from each ^{4}T term are at relatively similar energies (differences of less than 2 000 cm^{-1}), as shown in Figure 9. This observation reflects the modest distortions in the MO energies of these complexes from a typical octahedral splitting pattern of t_{2g} and e_g orbitals (Figure 8).

The quartet excited states of *trans*-[VCl$_2$(dmpe)$_2$] show important perturbations relative to those of *trans*-[VCl$_2$(tmeda)$_2$]. First, and as revealed in Figure 9, the components of the ^{4}T$_{2g}$, ^{4}T$_{1g}$(F), and ^{4}T$_{1g}$(P) parent states of *trans*-[VCl$_2$(dmpe)$_2$] are, on average, shifted to much higher energy (~18 100, 24 700, and 38 600 cm^{-1}) compared to *trans*-[VCl$_2$(tmeda)$_2$] (~11 500, 17 900, and 27 500 cm^{-1}). The higher-energy electronic transitions of *trans*-[VCl$_2$(dmpe)$_2$] are attributed to the stronger ligand-field imposed by the P donors for this complex, which increases 10Dq. Second, the individual components of the ^{4}T parent state of *trans*-[VCl$_2$(dmpe)$_2$] show larger energy differences within a given ^{4}T state. This observation is nicely illustrated in the plot of these states in Figure 9. For example, the ^{4}A$_g$ state from the ^{4}T$_{2g}$ parent term is ~6 000 cm^{-1} above the ^{4}B$_{3g}$ and ^{4}B$_{3g}$ states. On this basis, we tentatively assign the electronic absorption bands of *trans*-[VCl$_2$(dmpe)$_2$] at 13 900 cm^{-1} (720 nm) and 18 200 cm^{-1} (550 nm) to components of the ^{4}T$_{2g}$ parent term. The CASSCF/NEVPT2 calculations predict similar splitting patterns within the states of the ^{4}T$_{1g}$(F) and ^{4}T$_{1g}$(P) terms (Figure 9). Inspection of the configurations giving rise to these terms reveal that these differences are caused by the larger separation between the a$_g$(d$_{xy}$) and b$_{3g}$(d$_{yz}$)/b$_{2g}$(d$_{xz}$) MOs of complex *trans*-[VCl$_2$(dmpe)$_2$]. For example, the higher-energy ^{4}A$_g$ state (from ^{4}T$_{2g}$) involves excitation of an electron from the a$_g$(d$_{xy}$) MO to the b$_{1g}$(d$_{x^2-y^2}$) or a$_g$(d$_{z^2}$) MOs. In contrast, the lower-energy ^{4}B$_{3g}$ and ^{4}B$_{3g}$ states (from ^{4}T$_{2g}$) involve electron excitation from the b$_{3g}$(d$_{yz}$) or b$_{2g}$(d$_{xz}$) MOs to the b$_{1g}$(d$_{x^2-y^2}$) or a$_g$(d$_{z^2}$) MOs.

The CASSCF/NEVPT2 calculations predict a large number of doublet excited states, whose energies span the near-infrared to ultraviolet region of the energy spectrum (Table 2). We will focus our discussion on the lowest energy doublet states that derive from the ^{2}E$_g$ and ^{2}T$_{1g}$ terms in O_h symmetry. A comparison of the energies of these excited states is informative, as these states arise from the same electronic configuration as the ground state and thus are largely independent of 10Dq. In general, as noted above in the LFT section, the components of the ^{2}E$_g$

and $^2T_{1g}$ states of *trans*-[VCl$_2$(dmpe)$_2$] are lower in energy than those of *trans*-[VCl$_2$(tmeda)$_2$]. This difference likely reflects a reduction in electron-electron repulsion in the V^{II} center of *trans*-[VCl$_2$(dmpe)$_2$] due to the increased metal-ligand covalency of this complex (*i.e.*, a manifestation of the nephelauxetic effect[44]). The components of these terms for *trans*-[VCl$_2$(dmpe)$_2$] show more variation in energy, as was observed for the quartet terms. This variation can likewise be attributed to the relatively larger difference in energy between the a$_g$(d$_{xy}$) and b$_{3g}$(d$_{yz}$)/b$_{2g}$(d$_{xz}$) MOs in this complex.

The TD-DFT computations for *trans*-[VCl$_2$(tmeda)$_2$] and *trans*-[VCl$_2$(dmpe)$_2$] yielded energies for the components of the $^4T_{2g}$ and $^4T_{1g}$(F) excited states that are in quite good agreement with the CASSCF/NEVPT2 calculations (Table 2). For *trans*-[VCl$_2$(tmeda)$_2$], there are clusters of three transitions near ~14 000 cm^{-1} (~710 nm) and ~19 000 cm^{-1} (~530 nm). The relative energies of the components of the $^4T_{2g}$ term are the same in the TD-DFT and CASSCF/NEVPT2 computations, with the former being consistently higher in energy by 2 000 – 3 000 cm^{-1}. In contrast, the ordering differs slightly for the states derived from the $^4T_{1g}$(F) term, as the TD-DFT computations predict the $^4B_{1g}$ state at highest energy. There are larger discrepancies in the order of excited states between the TD-DFT and CASSCF/NEVPT2 calculations for the *trans*-[VCl$_2$(dmpe)$_2$] complex. However, the absolute difference between the excited state energies for these two computational methods is less than 2 500 cm^{-1}. We propose that the more covalent interactions in the *trans*-[VCl$_2$(dmpe)$_2$] complex and the similar energies between the components of the $^4T_{2g}$ and $^4T_{1g}$(F) terms makes this system more challenging to treat by the TD-DFT method.

Quantum Chemical Theory – Ground State Spin Hamiltonian Parameters from Electronic Structure Computations. The CASSCF/NEVPT2 calculations for *trans*-[VCl$_2$(tmeda)$_2$] and *trans*-[VCl$_2$(dmpe)$_2$] allow us to calculate zfs parameters for these complexes. Such calculations are useful for distinguishing contributions to zfs from spin-orbit coupling (D_{SOC}) and spin-spin coupling (D_{SSC}) mechanisms. The results are summarized in Table 3, which also compiles the experimental results.

The CASSCF/NEVPT2 calculations for *trans*-[VCl$_2$(tmeda)$_2$] predict $D = -0.34$ cm^{-1} and $|E/D| = 0.14$. The D value is dominated by the D_{SOC} term ($D_{SOC} = -0.27$ cm^{-1}), with the spin-spin coupling contribution only 20% of the total value ($D_{SSC} = -0.065$ cm^{-1}). The experimental and calculated D values differ by ~30% (Table 3), but this relative result can still be considered as

32

good agreement given that this corresponds to an absolute discrepancy of only ~0.8 cm^{-1}. More importantly, the negative sign of zfs is reproduced. The calculated g values are nearly isotropic and slightly below 2.0, as expected for a half-filled d shell: 1.963, 1.967, and 1.968 (g_{avg} = 1.966; close to the experimental value of 1.953(5)). The CASSCF/NEVPT2 calculations for *trans*-[VCl$_2$(dmpe)$_2$] predict D = +0.26 cm^{-1} and E/D = 0.017. These values are also in good agreement (within ~20%) with experiment (Table 3), and, as with the tmeda complex, the sign of D is reproduced, in this case positive. The D_{SOC} contribution is still dominant (D_{SOC} = 0.18 cm^{-1} and D_{SSC} = 0.08 cm^{-1}). The calculated g values are 1.978, 1.981, and 1.988 (g_{avg} = 1.982) – again, relatively uninformative in terms of being nearly isotropic and just below 2.0, exactly as found experimentally (g_{avg} = 1.989) and also what the above simple LFT analysis provided.

It is also possible to calculate the hyperfine coupling constants for ^{51}V and ^{14}N or ^{31}P as appropriate. The results are also summarized in Table 3. Unfortunately, the experimental data do not do justice to the calculations in terms of providing much corroboration. For the tmeda complex, the very small magnitude calculated (by both DFT and CASSCF/NEVPT2 methods) $\mathbf{A}(^{14}$N) is consistent with its lack of resolution by EPR and would be unlikely to be easily observed by ENDOR as well. In the dmpe complex, the $|\mathbf{A}(^{31}$P)| calculated by DFT is quite large (~50 MHz), although more than an order of magnitude smaller by CASSCF/NEVPT2. As noted above, it is discouraging that no ^{31}P ENDOR could observed; however, fluid solution EPR reported by Girolami et al.[1] is consistent with the DFT-calculated hyperfine coupling (see Table 3).

Table 3. Spin Hamiltonian parameters for *trans*-[VCl$_2$(tmeda)$_2$] and *trans*-[VCl$_2$(dmpe)$_2$].

Complex, Method	D (cm^{-1}), $|E/D|$	**g**, g_{avg}	**A**(^{51}V), A_{iso} (MHz)	**A**(^{14}N) or **A**(^{31}P), A_{iso} (MHz)
trans-[VCl$_2$(tmeda)$_2$]				
DFT	−0.22, 0.28	[1.983, 1.987, 1.987], 1.986	[−131.1, −134.3, −138.5], −134.6	[−2.04, −2.48, −2.51], −2.34
CASSCF/ NEVPT2	−0.34, 0.14	[1.963, 1.967, 1.968], 1.966	[−32.4, −0.46, −0.41], −11.09	[+1.72, +0.01, +0.01], +0.58
Expt. (HFEPR) [a]	−0.257(10), 0.082	[1.954(5), 1.944(6), 1.961(5)], 1.953	210(10)	Not observed
trans-[VCl$_2$(dmpe)$_2$]				
DFT	+0.47, 0.02	[1.994, 1.995, 1.995], 1.995	[−99.0, −110.7, −115.0], −108.2	[−48.3, −48.8, −53.4], −50.2
CASSCF/ NEVPT2	+0.26, 0.02	[1.978, 1.981, 1.988], 1.982	[+32.0, +23.2, +2.4], +19.2	[+7.4, +3.5, +1.9], +4.3
Expt. (HFEPR) [a]	+0.323(2), 0.20	[1.984(2), 1.989(3), 1.993(2)], 1.989	Not observed [b]	Not observed [b]

[a] The conventional EPR spectra recorded in frozen solution were consistent with the high precision spin Hamiltonian parameters extracted from HFEPR spectra (including $E = -0.021(7)$ and $+0.066(2)$ cm^{-1} for *trans*-[VCl$_2$(tmeda)$_2$] and *trans*-[VCl$_2$(dmpe)$_2$], respectively). No signs of hyperfine couplings can be determined from conventional EPR and only the $A_z(^{51}$V) component was determined, not the entire **A**(^{51}V) tensor, which is calculated. The other two components, $A_x(^{51}$V) and $A_y(^{51}$V), are likely axial and smaller (based on the EPR linewidths) so that using the DFT calculated A_{iso}: $\left(A_{\parallel} + 2A_{\perp} \right)/3 = A_{iso}; (-210 - 2\times97.5)/3 = -135$ MHz, thus, **A**(^{51}V) $\approx$ [−210, −97.5, −97.5] MHz is quite plausible for an estimate of the experimental ^{51}V hyperfine tensor.
[b] Girolami et al.[1] reported a room temperature (i.e., fluid toluene solution) X-band EPR spectrum of [VCl$_2$(dmpe)$_2$] that exhibited a 40-line pattern (as expected for fully separated ^{31}P and ^{51}V couplings: $\left(2n_P I_P + 1\right)\left(2n_V I_V + 1\right) = \left(2\times4\times\frac{1}{2}+1\right)\left(2\times1\times\frac{7}{2}+1\right) = 40$), which surprisingly, was not shown as a figure. This remarkable spectrum was analyzed to give $a(^{51}$V) = 237 MHz and $a(^{31}$P) = 75 MHz, both of which values are very roughly in the range calculated by DFT for this complex.

Conclusions

The class of complex *trans*-[VX$_2$(RR′ECH$_2$CH$_2$ERR′)$_2$] represents a key type of coordination geometry, namely tetragonally distorted octahedral 3d^3. This type of system has been explored early on for Cr^{III} analogs, but less so for V^{II}, and in particular not using state of the art computational methods, although a notable effort was made with what methods were available at the time.[18] We have previously studied such complexes with "bracketing" ions, namely 3d^2 Ti^{II} and 3d^4 Cr^{II}.[8, 26] Here we apply these techniques, both DFT and *ab initio*, making use of experimental results from paramagnetic resonance, both conventional EPR and HFEPR spectroscopy, as well as electronic absorption spectroscopy to provide a complete picture of the electronic structure of *trans*-[VCl$_2$(Me$_2$ECH$_2$CH$_2$EMe$_2$)$_2$] (E = N, P). This study highlights the key difference between N and P donors. Although this is not a new discovery in inorganic chemistry, it confirms this difference using quantitative experimental and theoretical techniques and focuses on the less studied metal ion, V^{II}. Both the LFT analysis and QCT computations allow us to conclude that the large difference in the electronic absorption spectra of *trans*-[VCl$_2$(tmeda)$_2$] and *trans*-[VCl$_2$(dmpe)$_2$] (Figure 2) has its origin in the larger splitting between the a$_g$(d$_{xy}$) and b$_{3g}$(d$_{xz}$)/b$_{2g}$(d$_{yz}$) MOs for the latter complex. In addition, by comparison to previous calculations for *trans*-[CrCl$_2$(dmpe)$_2$], we observe that the metal-dmpe π-covalency is strongly metal-dependent, as there is significantly more M-P covalency for M = Cr than M = V. It is also notable that the electronic differences between *trans*-[VCl$_2$(tmeda)$_2$] and *trans*-[VCl$_2$(dmpe)$_2$] is manifest in their zfs – relatively small in magnitude in both complexes compared to Ti^{II} or Cr^{II} analogs, but lesser and negative in the diamine while greater and positive in the diphosphine, with QCT reproducing this experimental result from, primarily, HFEPR. Collectively, this present work shows how traditional (LFT and AOM) and cutting-edge (CASSCF/NEVPT2) methods can be combined to understand transition metal electronic structure.

ASSOCIATED CONTENT

Supporting Information

Additional crystallographic and other structural comparative data, electronic absorption spectral data, details of experimental and computational methods, additional EPR spectra and diagrams; tables of results from LFT and QCT calculations.

AUTHOR INFORMATION

Corresponding Authors

Daniel J. Mindiola: mindiola@sas.upenn.edu
Timothy A. Jackson: taj@ku.edu
Joshua Telser: jtelser@roosevelt.edu

Notes

The authors declare no competing financial interests.

Dedication

We dedicate this paper to Prof. Peter T. Wolczanski, Cornell University, Ithaca, NY, USA on the occasion of his 70th birthday for his many contributions to inorganic and organometallic chemistry. The authors of Polish heritage and/or affinity wish him *sto lat*!

36

References

[1]   G. S. Girolami, G. Wilkinson, A. M. R. Galas, M. Thornton-Pett, M. B. Hursthouse, *J. Chem. Soc., Dalton Trans.* **1985**, 1339-1348.

[2]   G. S. Girolami, J. E. Salt, G. Wilkinson, M. Thornton-Pett, M. B. Hursthouse, *J. Am. Chem. Soc.* **1983**, *105*, 5954-5956.

[3]   J. A. Jensen, S. R. Wilson, A. J. Schultz, G. S. Girolami, *J. Am. Chem. Soc.* **1987**, *109*, 8094–8096.

[4]   R. J. Morris, G. S. Girolami, *Inorg. Chem.* **1990**, *29*, 4167–4169.

[5]   J. A. Jensen, G. S. Girolami, *Inorg. Chem.* **1989**, *28*, 2107–2113.

[6]   a J. J. H. Edema, R. Duchateau, S. Gambarotta, R. Hynes, E. Gabe, *Inorg. Chem.* **1991**, *30*, 154–156; b M. A. Araya, F. A. Cotton, J. H. Matonic, C. A. Murillo, *Inorg. Chem.* **1995**, *34*, 5424–5428.

[7]   G. B. Wijeratne, E. M. Zolnhofer, S. Fortier, L. N. Grant, P. J. Carroll, C.-H. Chen, K. Meyer, J. Krzystek, A. Ozarowski, T. A. Jackson, D. J. Mindiola, J. Telser, *Inorg. Chem.* **2015**, *54*, 10380-10397.

[8]   E. M. Zolnhofer, G. B. Wijeratne, T. A. Jackson, S. Fortier, F. W. Heinemann, K. Meyer, J. Krzystek, A. Ozarowski, D. J. Mindiola, J. Telser, *Inorg. Chem.* **2020**, *59*, 6187-6201.

[9]   M. A. Halcrow, *Dalton Trans.* **2020**, *49*, 15560-15567.

[10]   a J. J. H. Edema, W. Stauthamer, F. Van Bolhuis, S. Gambarotta, W. J. J. Smeets, A. L. Spek, *Inorg. Chem.* **1990**, *29*, 1302-1306; b D. G. L. Holt, L. F. Larkworthy, D. C. Povey, G. W. Smith, G. J. Leigh, *Inorg. Chim. Acta* **1993**, *207*, 11-19; c P. B. Hitchcock, D. L. Hughes, G. J. Leigh, J. R. Sanders, J. De Souza, C. J. McGarry, L. F. Larkworthy, *J. Chem. Soc., Dalton Trans.* **1994**, 3683-3687; d F. Süßmilch, F. Olbrich, H. Gailus, D. Rodewald, D. Rehder, *J. Organomet. Chem.* **1994**, *472*, 119-126; e P. B. Hitchcock, D. L. Hughes, L. F. Larkworthy, G. J. Leigh, C. J. Marmion, J. R. Sanders, G. W. Smith, J. S. de Souza, *J. Chem. Soc., Dalton Trans.* **1997**, 1127-1136.

[11]   R. J. Morris, S. R. Wilson, G. S. Girolami, *J. Organomet. Chem.* **1994**, *480*, 1-9.

[12]   S. J. Anderson, F. J. Wells, G. Willkinson, B. Hussain, M. B. Hursthouse, *Polyhedron* **1988**, *7*, 2615-2626.

[13]   P. Ghosh, H. Taube, T. Hasegawa, R. Kuroda, *Inorg. Chem.* **1995**, *34*, 5761-5775.

[14]   P. Frank, P. Ghosh, K. O. Hodgson, H. Taube, *Inorg. Chem.* **2002**, *41*, 3269-3279.

[15]   a J. P. Joyce, R. I. Portillo, A. K. Rappé, M. P. Shores, *Inorg. Chem.* **2022**, *61*, 6376-6391; b J. P. Joyce, R. I. Portillo, C. M. Nite, J. M. Nite, M. P. Nguyen, A. K. Rappé, M. P. Shores, *Inorg. Chem.* **2021**, *60*, 12823-12834.

[16]   a J. Krzystek, A. Ozarowski, J. Telser, *Coord. Chem. Rev.* **2006**, *250*, 2308-2324; b J. Telser, A. Ozarowski, J. Krzystek, in *Electron Paramagnetic Resonance: Volume 23, Vol. 23*, The Royal Society of Chemistry, **2013**, pp. 209-263.

[17]   A. C. Niedwieski, P. B. Hitchcock, J. D. d. Motta Neto, F. Wypych, G. J. Leigh, F. S. Nunes, *J. Braz. Chem. Soc.* **2003**, *14*, 750-758.

[18]   A. C. Niedwieski, J. F. Soares, G. Jeffery Leigh, F. S. Nunes, J. D. Da Motta Neto, *Int. J. Quantum Chem.* **2002**, *88*, 245-251.

[19]   M. M. Werst, C. E. Davoust, B. M. Hoffman, *J. Am. Chem. Soc.* **1991**, *113*, 1533-1538.

[20]   C. Mailer, C. P. S. Taylor, *Biochim. Biophys. Acta* **1973**, *322*, 195-203.

[21] A. K. Hassan, L. A. Pardi, J. Krzystek, A. Sienkiewicz, P. Goy, M. Rohrer, L.-C. Brunel, *J. Magn. Reson.* **2000**, *142*, 300-312.

[22] R. L. Belford, G. G. Belford, *J. Chem. Phys.* **1973**, *59*, 853-854.

[23] J. Bendix, in *Comprehensive Coordination Chemistry II, Volume 2: Fundamentals: Physical Methods, Theoretical Analysis, and Case Studies, Vol. 2* (Ed.: A. B. P. Lever), Elsevier, Amsterdam, **2003**, pp. 673-676.

[24] a F. Neese, *ORCA - an ab initio, Density Functional and Semiempirical Program Package*, *Version 4.0*, Max Planck Institute for Chemical Energy Conversion, 2017; b F. Neese, *Wiley Interdisciplinary Reviews: Computational Molecular Science* **2012**, *2*, 73-78.

[25] The room temperature structures gave (in Å): *trans*-[VCl$_2$(tmeda)$_2$], d(V-Cl) = 2.487(1), d(V-N) = 2.319(2); *trans*-[VCl$_2$(dmpe)$_2$], d(V-Cl) = 2.440(4), d(V-P) = 2.499(5).

[26] E. M. Zolnhofer, A. A. Opalade, T. A. Jackson, F. W. Heinemann, K. Meyer, J. Krzystek, A. Ozarowski, J. Telser, *Inorg. Chem.* **2021**, *60*, 17865-17877.

[27] These diamine ligand abbreviations are: dmeda = *N*,*N'*-dimethylethane-1,2-diamine (R = H, R' = Me); deeda = *N*,*N'*-diethylethane-1,2-diamine (R = H, R' = Et); dieda = *N*,*N'*-diisopropylethane-1,2-diamine (R = H, R' = iPr).

[28] J. Telser, in *eMagRes, Vol. 6*, John Wiley & Sons, Ltd, **2017**, pp. 207-233.

[29] a R. A. Kinney, C. T. Saouma, J. C. Peters, B. M. Hoffman, *J. Am. Chem. Soc.* **2012**, *134*, 12637-12647; b J. S. Anderson, G. E. Cutsail, III, J. Rittle, B. A. Connor, W. A. Gunderson, L. Zhang, B. M. Hoffman, J. C. Peters, *J. Am. Chem. Soc.* **2015**, *137*, 7803-7809; c H. Yang, J. Rittle, A. R. Marts, J. C. Peters, B. M. Hoffman, *Inorg. Chem.* **2018**, *57*, 12323-12330.

[30] N. X. Gu, P. H. Oyala, J. C. Peters, *J. Am. Chem. Soc.* **2020**, *142*, 7827-7835.

[31] N. X. Gu, P. H. Oyala, J. C. Peters, *J. Am. Chem. Soc.* **2018**, *140*, 6374-6382.

[32] a B. R. McGarvey, *J. Chem. Phys.* **1962**, *37*, 3020-3021; b B. R. McGarvey, *J. Chem. Phys.* **1964**, *41*, 3743-3758.

[33] J. C. Hempel, L. O. Morgan, W. B. Lewis, *Inorg. Chem.* **1970**, *9*, 2064-2072.

[34] a B. M. Hoffman, *Acc. Chem. Res.* **1991**, *24*, 164-170; b B. M. Hoffman, *Acc. Chem. Res.* **2003**, *36*, 522-529.

[35] a J. Krzystek, S. A. Zvyagin, A. Ozarowski, S. Trofimenko, J. Telser, *J. Magn. Reson.* **2006**, *178*, 174-183; b J. Telser, J. Krzystek, A. Ozarowski, *J. Biol. Inorg. Chem.* **2014**, *19*, 297-318.

[36] J. R. Perumareddi, *Coord. Chem. Rev.* **1969**, *4*, 73-105.

[37] C. J. Ballhausen, in *Introduction to Ligand Field Theory*, McGraw-Hill, New York, **1962**, pp. 99-103.

[38] D. S. McClure, in *Advances in the Chemistry of Coordination Compounds* (Ed.: S. Kirschner), Macmillan, New York, **1961**.

[39] W. A. Baker, Jr., M. G. Phillips, *Inorg. Chem.* **1966**, *5*, 1042-1046.

[40] C. E. Schäffer, *Struct. Bonding* **1968**, *5*, 68-95.

[41] S. Mossin, H. Weihe, A.-L. Barra, *J. Am. Chem. Soc.* **2002**, *124*, 8764-8765.

[42] M. Keeton, B. F.-C. Chou, A. B. P. Lever, *Can. J. Chem.* **1971**, *49*, 192-198.

[43] a T. J. Barton, R. C. Slade, *J. Chem. Soc., Dalton Trans.* **1975**, 650-657; b M. Gerloch, R. C. Slade, in *Ligand-Field Parameters*, Cambridge University Press, Cambridge, UK, **1973**; c A. J. Bridgeman, M. Gerloch, *Prog. Inorg. Chem.* **1997**, *45*, 179-281.

38

[44]   C. K. Jørgensen, *Prog. Inorg. Chem.* **1962**, *4*, 73-124.

39

For Table of Contents Only
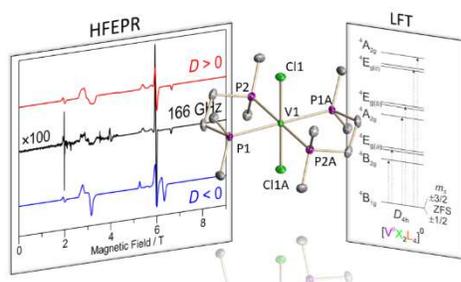
Synopsis

Two V^{II} ($3d^3$, $S = 3/2$) complexes of formula *trans*-[$VCl_2(Me_2ECH_2CH_2EMe_2)_2$] where E = N and P (thus tmeda and dmpe ligands) are studied by EPR, including high-frequency and -field EPR, and optical spectroscopy. Their electronic structure is described using both classical ligand-field theory (LFT) and state-of-the-art quantum chemical theory (QCT) including *ab initio* methods and highlights the differences between diamine and diphosphine ligands.

40